ADVANCES IN INORGANIC CHEMISTRY, VOL. 46

THE OCTAHEDRAL M_6Y_8 AND M_6Y_{12} CLUSTERS OF GROUP 4 AND 5 TRANSITION METALS

NICHOLAS PROKOPUK and D. F. SHRIVER

Department of Chemistry, Northwestern University, Evanston, Illinois 60208

I. Introduction

The early transition metal halide clusters $\{M_6Y_8\}^{n+}$ (M = Mo, W; Y = Cl, Br, I; M = Nb; Y = I) and $\{M_6Y_{12}\}^{n+}$ (M = Nb, Ta; Y = Cl, Br) are the basis for a diverse solid-state chemistry in which cluster fragments are interconnected by halide bridges. Discrete clusters containing the $\{M_6Y_8\}^{n+}$ and $\{M_6Y_{12}\}^{n+}$ units are obtained from these materials by addition of ligands that disrupt the halide bridges. Control of the coordination environment about the metal octahedron in the soluble clusters provides control of the chemical and physical properties

0898-8838/99 $25.00

of the cluster. In addition, the discrete clusters provide building blocks for the construction of new types of extended cluster arrays and cluster based materials.

Octahedral clusters of the electropositive metals, groups 3 to 7, are stabilized by π-donor ligands such as halides, chalcogenides, and alkoxides, but the majority accessible to solution chemistry are the halide complexes. These highly symmetric and aesthetically pleasing $\{M_6Y_8\}^{n+}$ and $\{M_6Y_{12}\}^{n+}$ clusters contain a robust core of six metal atoms and either 8 face-capping $\{M_6Y_8\}^{n+}$ or 12 edge-bridging $\{M_6Y_{12}\}^{n+}$ halide ligands Y. An additional 6 ligands X are terminally bound, one to each metal center, completing the structures $[M_6Y_8Y_6]^{n-6z}$ and $[M_6Y_{12}X_6]^{n-6z}$ (Fig. 1). In the present discussion it is convenient to refer to the charge of only the $\{M_6Y_8\}^{n+}$ or $\{M_6Y_{12}\}^{n+}$ unit instead of referring to the entire cluster and its full complement of axial ligands. This notation is especially useful when there is ambiguity as to the type and charge of the ligands occupying the axial sites or when the properties of the cluster core are independent of the axial ligands. Nomenclature developed by Schäfer and von Schnering (*1*) denotes the bridging ligands as inner (superscript i) and the terminal ligands outer (from *ausser*) or axial (superscript a); thus, $[Mo_6Cl_{14}]^{2-}$ is noted $[Mo_6Cl_8^iCl_6^a]^{2-}$. Soluble octahedral clusters $\{M_6Y_8\}^{n+}$ and $\{M_6Y_{12}\}^{n+}$ with inner halide ligands have been reported for Nb, Ta, Mo, and W. Molybdenum and tungsten are observed predominately in the $\{M_6Y_8\}^{n+}$ geometry, and the group 5 metals are found with the $\{M_6Y_{12}\}^{n+}$ arrangement. One notable exception is the niobium iodide clusters such as $[Nb_6I_8(NH_2CH_3)_6]$ in which the iodide ligands occupy face-capping sites on the Nb_6 octahedron (*2*).

Solid compounds with $\{M_6Y_8\}^{n+}$ or $\{M_6Y_{12}\}^{n+}$ units and halide ligands have been observed for other metals, including those of the rare earth

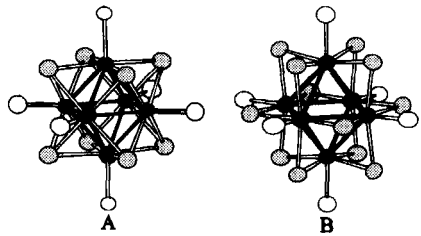

FIG. 1. Structures of $[M_6Y_8X_6]^z$ **A** and $[M_6Y_{12}X_6]^z$ **B**.

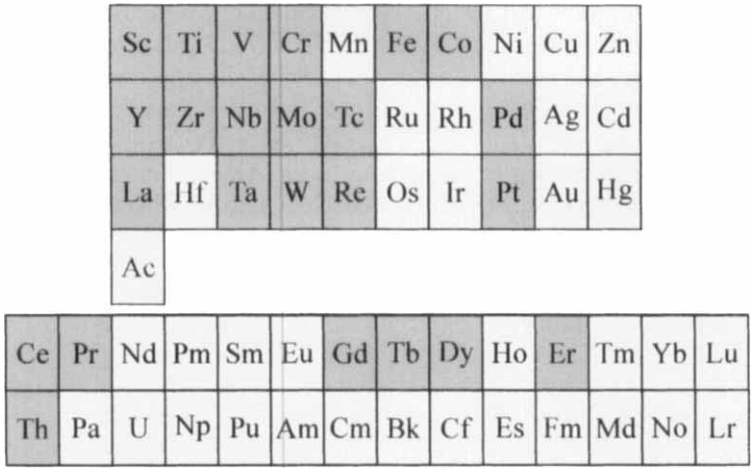

FIG. 2. Periodic table of metals (shaded) found in $\{M_6Y_8\}^{n+}$ or $\{M_6Y_{12}\}^{n+}$ geometry.

and late d-block elements (Fig. 2). Extensive intercluster bridging has confined the chemistry of the majority of these compounds to the condensed phases. By contrast, the weak intercluster bridging in the group 5 and 6 derivatives provides solid-state materials that are easily dissolved into molecular cluster species. Subsequent solution chemistry has revealed rich photophysical and redox properties for these compounds. The relationship between the ligation of the group 5 and 6 metal halide clusters and their chemical and physical properties, as well as the subsequent materials chemistry that has evolved from this association, is the subject of this review. The solid-state and solution chemistry of the related zirconium halide clusters $\{Zr_6Y_{12}\}^{n+}$, which occur with interstitial atoms occupying the center of the metal octahedron or hydrides ligands bridging the octahedron faces, is relatively new and has been the subject of a number of reviews (*3*, *4*).

II. Group 6

Recent interest in halide clusters containing the $\{M_6Y_8\}^{n+}$ unit stems in part from its structural relationship to the superconducting Chevral phases $PbMo_6Q_8$ (Q = S, Se, Te) in which eight chalcogenide ligands Q occupy the face-capping positions (*5*, *6*). Early development of the ligand substitution chemistry of the group 6 clusters had led to recent applications of these compounds to catalysis and materials

chemistry. Molybdenum(II) chloride was discovered over 100 years ago (*7*), and the related cluster $Mo_6Cl_8(OH)_4(H_2O)_2$ was one of the first complexes characterized by X-ray diffraction (*8*). Renewed interest in the substitution chemistry of the inner ligands arises from the promise of generating $\{Mo_6Q_8\}^{2-}$ (Q = S, Se, Te) units in solution, which are potential precursors to Chevral phases. Also of current interest is the discovery of the long-lived excited state exhibited by the molybdenum and tungsten clusters (*9*, *10*).

A. Synthesis of Group 6 Clusters

Early synthetic procedures for the group 6 metal halide clusters relied on disproportionation reactions of the intermediate halides, $MoCl_3$, $MoBr_3$, WCl_4, and WBr_4, at elevated temperatures to produce the clusters M_6X_{12} (*11*, *12*). These reactions suffered from inherently poor yields and the need to synthesize and isolate the reactive intermediate metal halide. McCarley and co-workers (*13*) introduced the use of sodium tetrahaloaluminate melts to reduce the halides MoX_5 and WX_6 (X = Cl, Br) with aluminum at lower temperatures:

$$6MoCl_5 + 6Al \rightarrow Mo_6Cl_{12} + 6AlCl_3 \quad (1)$$

$$6WCl_6 + 8Al \rightarrow W_6Cl_{12} + 8AlCl_3. \quad (2)$$

Near quantitative yields are achieved for the molybdenum halides, but substantially lower yields (50%) are obtained in the synthesis of the tungsten clusters, which require higher temperatures and the use of Vycor reaction vessels. A higher yield low-temperature synthesis was devised by McCarley and co-workers for W_6Cl_{12} using iron as the reducing agent (*14*).

The chemical reduction of the higher Mo and W halides provides good yields of the octahedral clusters, but the mechanism is obscure. By contrast, chemical oxidation of zero-valent Mo and W leads to the bromo and iodo cluster species in poor yields but provides considerable insight into the formation of these cluster compounds. The reaction of the hexacarbonyls $Mo(CO)_6$ or $W(CO)_6$ with I_2 at moderately low temperatures produces a mixture of metal halide phases (*15*, *16*). In the reaction $W(CO)_6$ with I_2, lower nuclearity clusters have been isolated as reaction intermediates that lead to W_6 species. The tri-, tetra-, and pentanuclear tungsten iodide species are obtained from $W(CO)_6$ and I_2 by varying reaction times and temperatures, and the

following reaction sequence was proposed by Franolic, Long, and Holm:

$$[W_3I_9]^{1-} \rightarrow [W_4I_{11}]^{1-} \rightarrow [W_5I_{13}]^{1-} \rightarrow [W_6I_{14}]^{2-}. \quad (3)$$

The lower nuclearity clusters $[Mo_5Cl_{13}]^{2-}$ were isolated from $MoCl_5$ in $AlCl_3/KCl/BiCl_3/Bi$ melts that led to the hexanuclear species (*17*). This is the only intermediate isolated from reaction mixture that produces the $\{Mo_6Cl_8\}^{4+}$ core. Solution chemistry has yielded Mo_2, Mo_3, and Mo_4 halide species from mononuclear molybdenum complexes, suggesting that a nucleation process similar to that proposed for the tungsten systems may take place during the formation of hexanuclear molybdenum clusters (*18–22*).

Extraction of the cluster from the products of the solid-state reactions with HX yields the hydronium salts of the molecular species $(H_3O)_2(M_6X_8X_6)\cdot 6H_2O$, which are converted into the polymeric material $M_6X_8^iX_2^aX_{4/2}^a$ under vacuum at 200°C (*12*, *23*). The structure of $M_6X_8^iX_2^aX_{4/2}^a$, also designated M_6X_{12}, consists of a $\{M_6X_8\}^{4+}$ core with two terminal axial ligands X_2^a and four axial ligands bridged to neighboring clusters $X_{4/2}^a$ (*11*) (Fig. 3). Both M_6X_{12} and $(H_3O)_2(M_6X_8X_6)\cdot 6H_2O$ may serve as precursors to new molecular species containing the metal halide cluster core $\{Mo_6X_8\}^{4+}$.

B. Axial Ligand Chemistry

The ligand substitution chemistry of the axial ligands of the group 6 clusters is considerably more developed than the substitution chem-

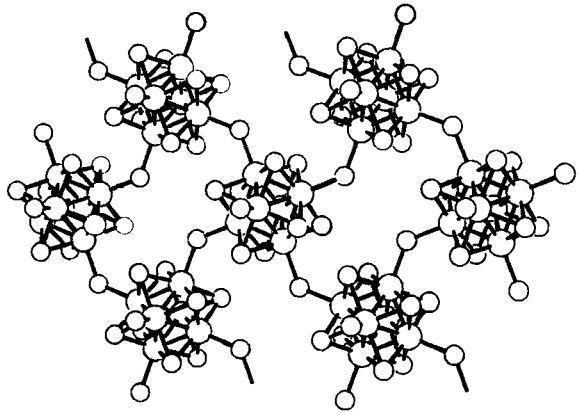

FIG. 3. Structure of $Mo_6Cl_8Cl_2Cl_{4/2}$. Reprinted with permission from Ref. (*130*).

istry of the inner ligands. This is due largely to the robust nature of the $\{M_6Y_8\}^{4+}$ core, which requires substantially harsher conditions to displace the inner ligands. The increased lability of the axial ligands enables the coordination environment about the $\{M_6Y_8\}^{4+}$ framework to be altered without disrupting the metal octahedron on the Y_8 cube.

1. Mechanism of Ligand Exchange

Kinetic studies of the ligand exchange reaction

$$[Mo_6Cl_8Cl_6]^{2-} + 6Br^- \rightarrow [Mo_6Cl_8Br_6]^{2-} + 6Cl^- \quad (4)$$

were performed by Sheldon with ^{36}Cl-labeled $[Mo_6Cl_8Cl_6]^{2-}$ in aqueous solutions. The rate-determining step was found to be first order with respect to the molybdenum cluster and independent of halide concentration, and hence the aquation step

$$[Mo_6Cl_8Cl_6]^{2-} + H_2O \rightarrow [Mo_6Cl_8Cl_5H_2O]^- + Cl^- \quad (5)$$

was proposed as rate limiting (*24*). Schäfer found similar results with the exchange reactions of $[Mo_6Cl_8Cl_6]^{2-}$ and $[W_6Cl_8Cl_6]^{2-}$ with Br^- and I^- (*25*). Two significant findings from Schäfer's work are the equivalency of the six axial positions and the rate dependence on the metal itself, which show that reactions of molybdenum clusters proceed faster than those of the analogous tungsten complexes.

Preetz substantiated the equivalency of the axial positions for the ligands F^-, Cl^-, Br^-, I^-, and NCS^- by monitoring the ^{19}F and ^{15}N and ^{95}Mo NMR spectra of the ligand exchange reactions

$$[Mo_6Cl_8F_6]^{2-} + [Mo_6Cl_8X_6]^{2-} \rightarrow [Mo_6Cl_8F_{6-n}X_n]^{2-} \quad X = Cl, Br, \text{ and } I \quad (6)$$

and

$$[Mo_6Cl_8(NCS)_6]^{2-} + [Mo_6Cl_8X_6]^{2-} \rightarrow [Mo_6Cl_8(NCS)_{6-n}X_x]^{2-} \quad X = F, Cl, Br, \text{ and } I. \quad (7)$$

Reaction rates were found to increase with the series $X = Cl < Br < I < SCN < F$, equilibration of the thiocyanate cluster was achieved in 10 h, and 2–3 days were required for the formation of the fluoride cluster at room temperature (*26, 27*). All the clusters $[Mo_6Cl_8F_{6-n}X_x]^{2-}$ and $[Mo_6Cl_8(NCS)_{6-n}X_n]^{2-}$ including structural isomers (i.e., *mer* or *fac* of $[Mo_6Cl_8F_3X_3]^{2}$) were identified by NMR. In all cases a statistical

distribution of all possible compounds, inclusive of the ratios for the structural isomers, was obtained. Importantly, no evidence of isomer-steering electronic effects was observed.

2. Synthesis of Molecular $\{M_6Y_8\}$ Clusters

Various types of neutral ligands, including nitrogen donors (*12*, *23*, *28*, *29*), oxygen donors (*12*, *28*, *30*, *31*), phosphines (*28*, *32*, *33*), and solvent molecules (*28*, *34*, *35*), disrupt the extended Mo_6Cl_{12} and W_6Cl_{12} solid structure. Under harsher conditions terminal chloride ligands of Mo_6Cl_{12} are displaced by neutral donor ligand, L:

$$Mo_6Cl_{12} + x\text{sL} \rightarrow [Mo_6Cl_8Cl_{4-x}L_{2+x}]^{x+} \tag{8}$$

For instance, addition of PPh_3 to Mo_6Cl_{12} yields $Mo_6Cl_8Cl_4(PPh_3)_2$ at room temperature, but it is necessary to reflux Mo_6Cl_{12} with an excess of PPh_3 in tetrahydrofuran to produce the triphosphine cluster $[Mo_6Cl_8Cl_3(PPh_3)_3]Cl$ (*28*). Similar experiments by Walton and co-workers with PEt_3 and Mo_6Cl_{12} in refluxing ethanol resulted in the reduced cluster $Mo_6Cl_8Cl_3(PEt_3)_3$, which contains a $\{Mo_6Cl_8\}^{3+}$ core. Magnetic susceptibility measurements conducted on $Mo_6Cl_8Cl_3(PEt_3)_3$ indicate that the cluster is diamagnetic, a result inconsistent with the expected odd number of electrons in the $\{Mo_6Cl_8\}^{3+}$ core. The compound was subsequently reformulated as the reduced species $[Mo_6Cl_8(PEt_3)_6]^{2+}$, which crystallizes with the counteranion $[Mo_6Cl_8Cl_6]^{2-}$ (*32*). The introduction of two triphenyl phosphine ligands increases the lability of the remaining chloride ligand in the biphosphine cluster $Mo_6Cl_8Cl_4(PPh_3)_2$. Both ethanol and pyridine dissolve Mo_6Cl_{12}, forming the solvent complexes $Mo_6Cl_8Cl_4(\text{solvent})_2$, but dissolution of the biphosphine cluster $Mo_6Cl_8Cl_4(PPh_3)_2$ in these solvents to leads to the species $[Mo_6Cl_8Cl_2(PPh_3)_2(HOEt)_2]^{2+}$ and $[Mo_6Cl_8Cl_2(PPh_3)_2(py)_2]^{2+}$ (*28*).

Neutral clusters with the formula $Mo_6Cl_8Cl_4L_2$ can exist as *cis* or *trans* isomers. Differences in polarity of the *cis* and *trans* structures were employed by Saito and co-workers to separate the isomers of $[Mo_6Cl_8Cl_4(P(n\text{-}C_3H_7)_3]_2$ by chromatography to produce 3 and 15% yields of the *cis* and *trans* respectively (*33*). The less polar *trans* isomers of $Mo_6Cl_8Cl_4(PR_3)_2$ (R = n-C_4H_9, n-C_5H_{11}) have also been isolated in greater than 40% yields (Fig. 4). Shifts in the ^{31}P NMR spectra reveal a preference for the formation of the all-*trans* isomer. DiSalvo and co-workers effected the isomerization of *trans*-$Mo_6Cl_8Cl_4[P(n\text{-}C_5H_{11})_3]_2$ into *cis*-$Mo_6Cl_8Cl_4[P(C_2H_5)_3]_2$ by immersing the *trans*-$P(n\text{-}C_4H_{11})_3$ cluster in a THF solution of $P(C_2H_5)_3$ (Fig. 5). A 95% conversion

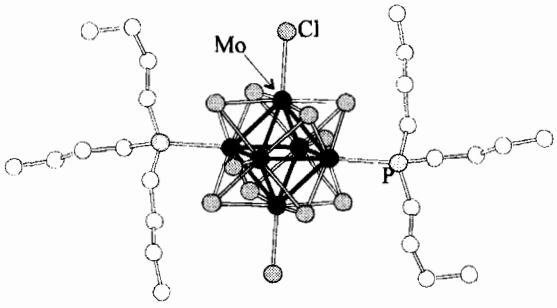

FIG. 4. Structure of *trans*-$Mo_6Cl_8Cl_4[P(n\text{-}C_4H_9)_3]_2$.

to the *cis* isomer was obtained (*36*). Alkylation of the *trans* phosphine clusters $Mo_6Cl_8Cl_4(PR_3)_2$ with trialkylaluminum reagents AlR'_3 (R′ = CH_3, C_2H_5, *n*-C_3H_7, *n*-C_4H_9, and *n*-C_6H_{13}) leads to the replacement of two axial chloride ligands with R groups, $Mo_6Cl_8Cl_2(PR_3)_2$ $(R')_2$ (Fig. 6). Additional AlR'_3 reacts with $Mo_6Cl_8Cl_2(PR_3)_2(R')_2$ producing the trialkyl $Mo_6Cl_8Cl(PR_3)_2(R')_3$, and both *mer* and *fac* isomers were shown to be present by ^{31}P NMR. These organometallic derivatives are the only examples in which carbon atoms are directly bound to the metal atoms of the $\{Mo_6Cl_8\}^{4+}$ framework.

Addition of two equivalents of sodium methoxide to Mo_6Cl_{12} in methanol leads to $[Mo_6Cl_8Cl_4(OCH_3)_2]^{2-}$ (*37*). Single-crystal X-ray diffraction reveals that the methoxide ligands occupy axial positions in a *trans* geometry (Fig. 7). However, it is not clear whether the *trans*

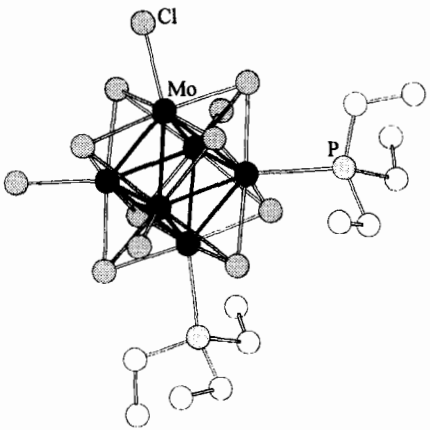

FIG. 5. Structure of *cis*-$Mo_6Cl_8Cl_4[P(C_2H_5)_3]_2$.

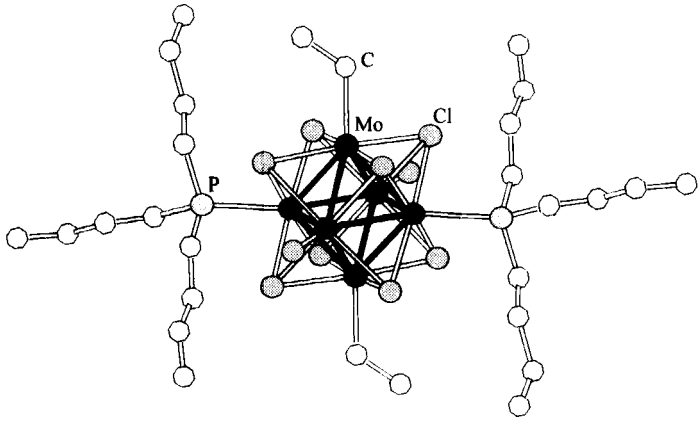

FIG. 6. Structure of all-*trans*-$Mo_6Cl_8Cl_2(C_2H_5)_2[P(C_2H_5)_3]_2$.

isomer is formed exclusively or only crystallizes preferentially because neither solution NMR nor X-ray powder pattern data on the bulk material was reported. In contrast to the bisphosphine clusters $Mo_6Cl_8Cl_4(PR_3)_2$, in which both electronic and steric factors may affect the *cis/trans* ratio of the products, only electronic effects are likely to influence the formation of the *trans* isomer of $[Mo_6Cl_8Cl_4(OCH_3)_2]^{2-}$. The *trans* isomer of $[Mo_6Cl_8Cl_4Br_2]^{2-}$ was prepared from crystalline $Mo_6Cl_8Cl_4(H_2O)_2$ in a heterogeneous reaction with Br^-. Homogeneous mixtures of $Mo_6Cl_8Cl_4(H_2O)_2$ and LiBr/$[(C_6H_5)_4As]Br$ lead to bromide-rich clusters $[(C_6H_5)_4As]_2[Mo_6Cl_8Cl_{1.2}Br_{4.8}]$ after only 30 min (*35*).

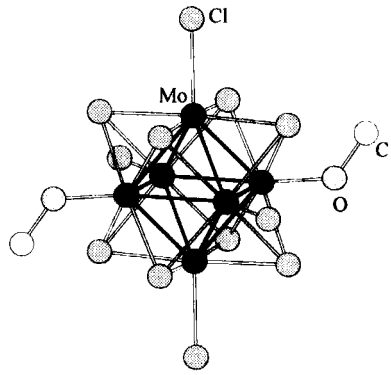

FIG. 7. Structure of *trans*-$[Mo_6Cl_8Cl_4(OCH_3)_2]^{2-}$.

Mixed halo clusters $(H_3O)_2M_6Cl_8Y_6$ (M = Mo, W; Y = F, Br, I) have been prepared from the aqueous acids HY and Mo_6Cl_{12} (*12*, *27*, *32*, *35*). It is likely the substitution results from an excess of the acid, HX, rather than the relative affinities of the $\{Mo_6Cl_8\}^{4+}$ core for the halide, X^-, ions. Dehydration of $(H_3O)_2[M_6Cl_8Y_6]$ leads to the mixed ligand bridged systems $Mo_6Cl_8Y_2Y_{4/2}$, which are analogous in structure and reactivity to Mo_6Cl_{12} in that addition of 2L produces $Mo_6Cl_8Y_4L_2$. One of the first comparative studies of the mixed halide clusters $Mo_6Cl_8Y_2Y_{4/2}$ (Y = Cl, Br, and I) revealed that the axial iodide ligands of $Mo_6Cl_8I_2I_{4/2}$ are more susceptible to displacement by nitrobenzene than the terminal bromide or chloride lands of $Mo_6Cl_8Y_2Y_{4/2}$ (Y = Cl, Br) (*23*). Dissolution of $Mo_6Cl_8I_2I_{4/2}$ in nitrobenzene produces $[Mo_6Cl_8I_3(NO_2C_6H_5)_3]I$, and the bromo and chloro derivatives yield bisnitrobenzene complexes $Mo_6Cl_8Y_4(NO_2C_6H_5)_2$.

Strongly basic anions such as hydroxide and alkoxide easily displace the axial chloride ligands of $[Mo_6Cl_8Cl_6]^{2-}$; thus, titration of $[Mo_6Cl_8Cl_6]^{2-}$ with OH^- initially precipitates the tetrahydroxo cluster $Mo_6Cl_8(OH)_4(H_2O)\cdot 14H_2O$, which redissolves as the hexahydroxo cluster $[Mo_6Cl_8(OH)_6]^{2-}$ with increasing pH (*23*). Similarly, when Mo_6Cl_{12} is refluxed with sodium alkoxides in alcohol solution, the alkoxide substitutes for all of the axial chloride ligands (*35*, *39*). Methoxide, ethoxide, and pentafluorophenoxide clusters $[Mo_6Cl_8(OR)_6]^{2-}$ have also been generated by this method (*35*, *38*).

Increased lability of the axial positions has been achieved by introducing weakly coordinating ligands such as triflate (trifluoromethanesulfonate) (*40*, *41*), tetrafluoroborate (*26*, *42–45*), nitrate (*43*, *46*, *47*) tosylate (*40*), trifluoroacetate (*40*, *48*), and perchlorate (*34*). (*Caution: perchlorate complexes are hazardously explosive.*) Reactions of the chloro cluster $[Mo_6Cl_8Cl_6]^{2-}$ with the silver salt or the protonated form of the weakly coordinating base B^- generate the reactive species $[Mo_6Cl_8B_6]^{2-}$:

$$[Mo_6Cl_8Cl_6]^{2-} + 6AgB \rightarrow [Mo_6Cl_8B_6]^{2-} + 6AgCl(\downarrow) \quad (9)$$

$$[Mo_6Cl_8Cl_6]^{2-} + 6HB \rightarrow [Mo_6Cl_8B_6]^{2-} + 6HCl(\uparrow). \quad (10)$$

Only the axial chloride ligands were abstracted by the silver salts or acids, leaving the inner ligands and the $\{Mo_6Cl_8\}^{4+}$ core intact. The weakly coordinating ligands are easily displaced by anionic, X^-, or neutral ligands, L, generating the hexasubstituted clusters $[Mo_6Cl_8X_6]^{2-}$ or $[Mo_6Cl_8L_6]^{4+}$. Cotton and Curtis first employed this strategy with $AgClO_4$ to prepare the first tetracationic clusters with

the $\{Mo_6Cl_8\}^{4+}$ unit, $[Mo_6Cl_8(solvent)_6](ClO_4)_4$ (solvent = DMF or DMSO) (*34*). These compounds demonstrate the utility of using weakly coordinating ions to alter the coordination environments about the $\{Mo_6Cl_8\}^{4+}$ core, but they are potentially explosive.

The triflate derivative $[Mo_6Cl_8(OSO_2CF_3)_6]^{2-}$ (Fig. 8), has been used extensively in our laboratory to prepare new cluster derivatives with neutral ligands not previously observed to bind to the $\{Mo_6Cl_8\}^{4+}$ core in all six axial positions. Limits of the substitutional lability of the triflate ligand of $[Mo_6Cl_8(OSO_2CF_3)_6]^{2-}$ have been explored with ^{19}F NMR (*49*). Diagnostic shifts in the ^{19}F NMR signal of coordinated and uncoordinated (free) $OSO_2CF_3^-$ may be employed to monitor the displacement reactions. As expected, only one peak is observed in the ^{19}F NMR spectrum of $[Mo_6Cl_8(OSO_2CF_3)_6]^{2-}$ in noncoordinating methylene chloride. Two peaks are observed with THF, acetonitrile, and acetone, suggesting incomplete substitution of the triflate ligand by solvent molecules. A single peak is observed for $[Mo_6Cl_8(OSO_2CF_3)_6]^{2-}$ in both DMSO and methanol, indicating that the triflate ligands are completely displaced in these solvents (*49*). Titration of $[Mo_6Cl_8(OSO_2CF_3)_6]^{2-}$ in methylene chloride with phosphine ligands PR_3 (R = Et, *t*-butyl, Ph) generates all possible species $[Mo_6Cl_8(OSO_2CF_3)_{6-x}(PR_3)_x]^{(2-x)-}$ $(0 \leq x \leq 6)$ as determined by ^{31}P NMR. Unlike the ligand exchange reactions between $[Mo_6Cl_8F_6]^{2-}$ and $[Mo_6Cl_8Y_6]^{2-}$ (Y = Cl, Br, I, and NCS), in which a statistical distribution of products was formed (*26*, *27*), the $x = 2$ species is disfavored in the phosphine titration reactions. This may be due in part to the polar CH_2Cl_2 solvent, which may disfavor the neutral species. Interestingly species

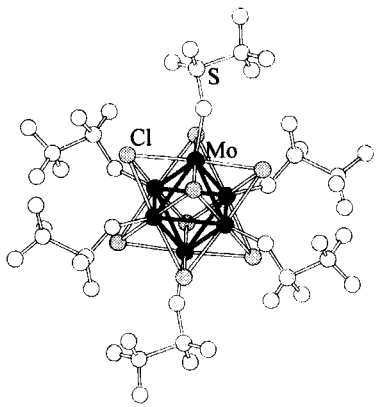

FIG. 8. Structure of $[Mo_6Cl_8(OSO_2CF_3)_6]^{2-}$.

with $x < 6$ persist in the presence of excess of the phosphines $P[C(CH_3)_3]_3$ and $P(C_2H_5)_3$ (*49*). It is unclear whether steric or electronic factors prevent full substitution of the triflate ligands by the phosphines.

The acetonitrile ligated cluster $[Mo_6Cl_8(NCCH_3)_6]^{4+}$ is an even more labile cluster than $[Mo_6Cl_8(OSO_2CF_3)_6]^{2-}$. DiSalvo and co-workers prepared the hexaacetonitrile complex as the $[SbCl_6]^-$ salt by treating $[Bu_4N]_2[Mo_6Cl_8(OSO_2CF_3)_6]$ with KSH to generate $[Bu_4N]_2[Mo_6Cl_8(SH)_6]$, which reacts with $SbCl_5$ in CH_3CN to produce $[Mo_6Cl_8(NCCH_3)_6][SbCl_6]_4$ in less than 5% yield (*50*). Some decomposition of the $\{Mo_6Cl_8\}^{4+}$ core is required to provide the sixth chlorine atom for the formation of the $[SbCl_6]^-$ counteranion. A similar abstraction of inner chloride ligands may have occurred in the alkylation reactions of the phosphine clusters $Mo_6Cl_8Cl_4(PR_3)_2$ with trialkyl aluminum reagents studied by Saito (*33*). The $[Mo_6Cl_6(NCCH_3)_6]^{4+}$ cation also can be prepared in near quantitative yield by reaction of the azide ligands of $[Mo_6Cl_8(N_3)_6]^{2-}$ with NO^+ in acetonitrile; however, the CH_3CN ligands are removed under vacuum and the BF_4^- ions then bridge molybdenum centers to fill the coordination sphere of the $\{Mo_6Cl_8\}^{4+}$ units (*49*).

The methoxide derivatives $[Mo_6Cl_8(OCH_3)_6]^{2-}$ and $[Mo_6Cl_8Cl_4(OCH_3)_2]^{2-}$ provide an alternative strategy for generating new clusters with the $\{Mo_6Cl_8\}^{4+}$ core (*51–55*). The strongly basic OCH_3^- ions are easily abstracted by Bronsted acids, liberating methanol. Nannelli *et al.* (*54*) first demonstrated the lability of the methoxide ligands with metathesis reactions between $[Mo_6Cl_8(OCH_3)_6]^{2-}$ and phenol:

$$[Mo_6Cl_8(OCH_3)_6]^{2-} + 6C_6H_5OH \rightarrow [Mo_6Cl_8(OC_6H_5)_6]^{2-} + 6HOCH_3. \quad (11)$$

The *trans* isomer of $[Mo_6Cl_8(OCH_2Ar)_6]^{2-}$ (Ar = 9-anthracenemethanol) was prepared from *trans*-$[Mo_6Cl_8Cl_4(OCH_3)_2]^{2-}$ (Fig. 9), indicating that little or no isomerization or ligand exchange between clusters occurs (*37*). This strategy is convenient in that readily available proton sources including alcohols, phenols, thiols, and carboxylic acids can be used, and the only by-products are solvent molecules. Other organic ligands with pK_a values comparable to phenol, such as sulfanamides, benzamide, pentafluoroanaline, acetylacetonate, and nitromethane, do not undergo the expected metathesis reactions with $[Mo_6Cl_8(OCH_3)_6]^{2-}$ (*56*). Interestingly, the hexaphenoxide derivative $[Mo_6Cl_8(OC_6H_5)_6]^{2-}$ reacts with benzoic acid to produce the benzoate cluster:

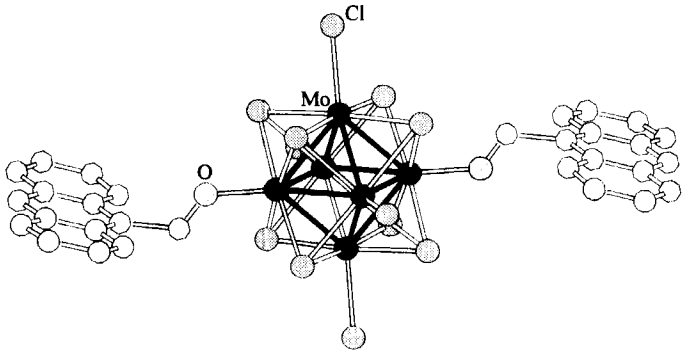

FIG. 9. Structure of *trans*-$[Mo_6Cl_8Cl_4(OCH_2C_{14}H_9)_2]^{2-}$.

$$[Mo_6Cl_8(OC_6H_5)_6]^{2-} + HO_2CC_6H_5 \rightarrow [Mo_6Cl_8(O_2CC_6H_5)_6]^{2-} + HOC_6H_5. \quad (12)$$

However, no reaction is observed between $[Mo_6Cl_8(OC_6H_5)_6]^{2-}$ and sodium benzoate, suggesting that formation of the alcohol or phenol is the driving force for these reactions (*56*).

C. Inner Ligand Chemistry

1. Mechanism of Ligand Exchange

Substitution of the inner ligands of $\{Mo_6Cl_8\}^{4+}$ and $\{W_6Cl_8\}^{4+}$ clusters requires more forcing conditions than those used to exchange axial ligands. Neither boiling *aqua regia* nor fuming sulfuric acid affect the $\{Mo_6Cl_8\}^{4+}$ core (*57*). Basic solutions, however, disrupt the cubic array of inner ligands. The inner halide ligands of $[Mo_6Cl_8(OH)_6]^{2-}$ and $[Mo_6Br_8(OH)_6]^{2-}$ are susceptible to partial displacement by hydroxide ions, $[Mo_6X_{8-z}(OH)_z(OH)_6]^{2-}$. Kinetic studies of the substitution of the inner chloride and bromide ligands by OH^- reveal that the process occurs with a second-order rate law, which is first order with respect to both cluster and the hydroxide ion. Interestingly, substitution of the bromide ligands of $[Mo_6Br_8(OH)_6]^{2-}$ by OH^- was found to be autocatalytic, suggesting that steric factors play a role in displacement of the bromides (*58*, *59*).

2. Inner Ligand Exchange

As implied in the previous discussion, the inner ligands have lower lability than their outer counterparts, but full substitution of the in-

ner chloride ligands by methoxide ions can be effected by boiling solutions of sodium methoxide and Mo_6Cl_{12} to dryness. The resulting cluster, $Na_2[Mo_6(OCH_3)_8(OCH_3)_6]$, which has face-capping methoxide ions, is pyrophoric (*39*, *60*).

Brückner *et al.* prepared mixed inner ligand species by heating the mixed halide clusters $Mo_6Cl_8X_2X_{4/2}$ (X = Br, I) to 400°C (*44*, *45*). The resulting mixtures of clusters were converted to the fluoride derivatives $[Bu_4N]_2[Mo_6(Y_zCl_{8-z})F_6]$ and analyzed by NMR spectroscopy. Deconvolution of the 1D and 2D ^{19}F NMR spectra revealed a mixture of products and structural isomers, all of which were identified in the NMR spectra. A statistical distribution of products is obtained from $Mo_6Cl_8Br_2Br_{4/2}$. A contrasting result was observed when $Mo_6Cl_8I_2I_{4/2}$ was heated to produce the $z = 3$ and 4 species as the most abundant species. Complexes containing iodide ligands in close proximity are favored. Complete exchange of both inner and outer chloride ligands of $M_6Cl_8Cl_2Cl_{4/2}$ (M = Mo, W) occurs in fused salt mixtures of LiX/KX (X = Br, I) (*12*, *61*).

The similarity between the structure of $\{Mo_6Cl_8\}^{4+}$ and the Mo_6Q_8 (Q = chalcogenide) unit of the superconducting Chevral phases has stimulated interest in the substitution chemistry of the inner ligands and, in particular, substitution of the inner chloride ligands by a chalcogenide. A number of mixed halide–chalcogenide clusters $\{Mo_6(Y_{8-z}Q_z)\}$ (X = Cl, Br, I; Q = S, Se, Te; z = 1, 3, 4, 6, 8) have been prepared from $Mo_6Cl_8Cl_2Cl_{4/2}$ and the elemental chalcogenide at elevated temperatures (900°C) (*62–64*). The clusters are linked into extended arrays through both inner and outer bridging ligands $\{Mo_6(Y_{8-z}Q_z)\}$ (Fig. 10). Diamagnetic and dielectric properties of these solids reveal insulator to metal to superconductor transitions upon increasing chalcogenide content, halide size, and intercluster bridging.

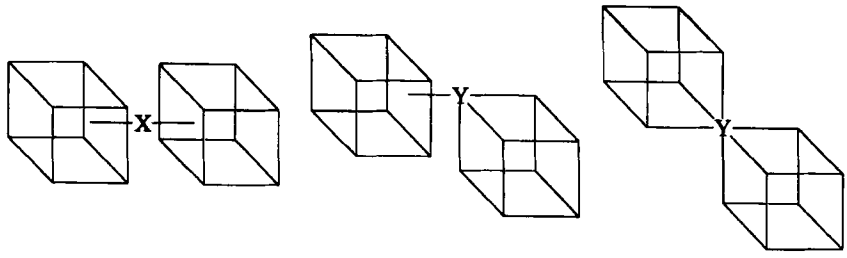

FIG. 10. Intercluster bridging between $\{M_6Y_8\}^{n+}$ clusters. The vertices of the cube represent the inner ligands Y.

Lower temperature methods for introducing chalcogenides into the face-capping positions of Mo_6Cl_{12} were developed in McCarley's laboratory, where Mo_6Cl_{12} in pyridine was refluxed with NaSH. The resulting soluble mixed-capped cluster $(pyH)_3[Mo_6(Cl_7S)Cl_6]$ was obtained in 41% yield (*65*). Saito used similar conditions followed by extensive chromatographic separation to prepare the mixed halide–chalcogenide clusters $[Mo_6(Y_7Q)X_6]^{3-}$ (X = Y = Cl, Br; Q = S, Se) and the disubstituted species $[Mo_6(Cl_6Se_2)Cl_6]^{3-/4-}$ (*66*, *67*). The chemistry of these interesting chalcogenide clusters has not been pursued. The observation that chromatography of the clusters with a chloride-deficient eluent produces the aqua complex $[Mo_6(Cl_7Q)(H_2O)_6]^{3+}$ indicates that the axial chloro ligands of the chalcogenide-doped clusters are more labile than those of the all-chloro complex $[Mo_6Cl_8Cl_6]^{2-}$.

Tungsten clusters with inner halide–chalcogenide ligands have been prepared by the reaction of W_6Cl_{12} and A_2Se (A = Na, K) (*68*). When W_6Cl_{12} and an alkali metal chalcogenide are refluxed in toluene with triethyl phosphine, clusters with mixed ligands are produced, $[W_6(Se_zCl_{8-z})(PEt_3)_6]^{1+}$ (z = 7.0, A = Na; z = 6.4, A = K). Slight changes in reaction conditions or chalcogenide source significantly affect the halide/chalcogenide ratio of the substituted product.

Full substitution of the inner chloride ligands of both Mo_6Cl_{12} and W_6Cl_{12} by chalcogenides produce molecular clusters with the $\{M_6Q_8\}^{n+}$ cores. When W_6Cl_{12} and elemental sulfur are heated to 300°C, an uncharacterized cluster results, which reacts with magnesium in the presence of triethylphosphine to generate $W_6S_8(PEt_3)_6$ in 10% yield (*69*). Better yields for $\{M_6S_8\}^{n+}$ (M = Mo, W) are obtained when M_6Cl_{12}, NaSH, and NaOBu are refluxed in pyridine. In these reactions the NaOBu serves as a proton abstractor and the chalcogenide clusters are isolated as the pyridine adducts (*14*, *70*, *71*). The chemistry and structural variations of the group 6 metal chalcogenide clusters were recently reviewed in this series, and the reader is referred to this publication for further information on these compounds (*72*).

D. Redox Chemistry and Photophysics of the Group 6 Metal Halide Clusters

The robust nature of the $\{Mo_6Cl_8\}^{4+}$ core in combination with its photophysical and redox properties is ideal for solar energy storage (*73*). Voltammetry on $[Mo_6Cl_8Cl_6]^{2-}$ in acetonitrile reveals two 1-electron steps at −1.53 and 1.56 V (vs SCE), corresponding to generation of the oxidized and reduced species $[Mo_6Cl_8Cl_6]^{1-}$ and $[Mo_6Cl_8Cl_6]^{3-}$, respectively (*74*). Electrolysis of $[Mo_6Cl_8Cl_6]^{2-}$ at potentials more posi-

tive than that of the 2−/1− couple generates the oxidized cluster $[Mo_6Cl_8Cl_6]^{1-}$, with no evidence for decomposition or any new electroactive species (*75*). Coulometric measurements are consistent with quantitative one-electron oxidation of the cluster; however, the oxidized species $[Mo_6Cl_8Cl_6]^{1-}$ with a $\{Mo_6Cl_8\}^{5+}$ core was not isolated (*10*). Voltammetry experiments on $[Mo_6Cl_8Cl_6]^{2-}$ in basic chloroaluminate melts reveal a reversible oxidation couple corresponding to generation of $[Mo_6Cl_8Cl_6]^{1-}$. In contrast to the voltammetry experiments in acetonitrile, the $[Mo_6Cl_8Cl_6]^{2-}/[Mo_6Cl_8Cl_6]^{3-}$ couple in the ionic melt is chemically irreversible, presumably due to dissociation of axial chloride ligands (*76*). The oxidized clusters $[M_6Y_8X_6]^{1-}$ (M = Mo, W; Y = Cl, Br, I; X = Cl, Br, I) with the $\{M_6X_8\}^{5+}$ core have been generated electrochemically in organic electrolytes (Table I) (*10*, *77*, *78*).

The tungsten clusters $[W_6Y_8X_6]^{1-}$ (X, Y = Cl, Br) have been produced by chemical oxidation of $[W_6Y_8X_6]^{2-}$ with NO^+ (*79*). Oxidation of W_6Br_{12} with liquid bromine in a net two-electron process, and the extended structure, $W_6Br_8Br_4(Br_4)_{2/2}$, results consisting of $\{W_6Br_8\}^{6+}$ units bridged in a linear array by $(Br_4)^{2-}$ anions (*80*, *81*). The rearrangement of inner halide ligands to edge-bridging positions takes place with $W_6Cl_8Cl_2Cl_{4/2}$ at elevated temperatures in the presence of chlorine (*82*). The resulting core $\{W_6Cl_{12}\}^{6+}$ contains 12 edge-bridging chloride ligands, and 6 axial chlorides complete the structure of $W_6Cl_{12}Cl_6$. An alternative route to $W_6Cl_{12}Cl_6$ employs octachlorocyclopentene, C_5Cl_8, as both the oxidant and the chloride source (*83*). Oxidation of $Mo_6Cl_8Cl_2Cl_{4/2}$ by C_5Cl_8 leads to $Mo_6Cl_{12}Cl_3$, which can be converted to the tetraethylammonium salt of $[Mo_6Cl_{12}Cl_6]^{3-}$ (*83*). The clusters $W_6Cl_{12}Cl_6$ and $[Mo_6Cl_{12}Cl_6]^{3-}$ are the only known examples of

TABLE I

REDOX POTENTIALS[a] FOR SOME $\{M_6Y_8\}^{n+}$ CLUSTERS

Cluster	$E_{1/2}$ (Ox)	$E_{1/2}$ (Red)	Reference
$[Mo_6Cl_8Cl_6]^{2-}$	1.60	−1.56	*10*
$[Mo_6Br_8Br_6]^{2-}$	1.38		*10*
$[W_6Cl_8Cl_6]^{2-}$	1.14		*10*
$[W_6Cl_8Br_6]^{2-}$	0.99		*78*
$[W_6Br_8Cl_6]^{2-}$	0.93		*77*
$[W_6Br_8Br_6]^{2-}$	0.80		*78*
$[W_6I_8I_6]^{2-}$	0.57		*78*
$[W_6I_8Br_6]^{2-}$	0.56		*78*

[a] All values were obtained from voltammetry experiments in CH_3CN and are referenced to SCE.

group 6 metal halide clusters adopting the $\{M_6Y_{12}\}^{n+}$ geometry. Conversion of the $\{M_6Y_8\}^{4+}$ core to $\{M_6Y_{12}\}^{n+}$ has only been observed in these reactions, and no examples are known in which the reverse transformation from $\{M_6Y_{12}\}^{n+}$ to $\{M_6Y_8\}^{4+}$ occurs.

Clusters containing chalcogenide ligands $\{Mo_6(Cl_{8-z}Q_z)\}^{n+}$ are somewhat more substitutionally labile than the all-halo complexes and undergo oxidation at potentials about 0.87 V less positive than that needed to oxidize the parent perhalo cluster (Table 1). The oxidation potentials of the chalcogenide-substituted clusters change very little with the identity of the chalcogenide, but significant solvent dependence is observed for the chalcogen-containing clusters. The cyclic voltammograms of $[Mo_6(Cl_7S)Cl_6]^{2-}$ in the noncoordinating solvent methylene chloride reveal a quasi-reversible wave corresponding to reduction of the cluster at 0.14 V vs. the ferrocene/ferrocenium couple. In acetonitrile this wave is shifted to 0.28 V, indicating that partial substitution of the axial ligands by CH_3CN has occurred. New waves grow in upon changing the potential on acetonitrile solutions of $[Mo_6(Cl_7S)Cl_6]^{2-}$, suggesting that further changes in the coordination environment of the $\{Mo_6(Cl_7S)\}^{n+}$ core take place upon switching the oxidation state of the cluster (*66*, *84*).

In the early 1980s Gray and co-workers discovered an unusually long-lived excited-state lifetime, 180 μs, for the cluster anion $[Mo_6Cl_8Cl_6]^{2-}$. The emission spectrum is substantially red shifted from the absorption bands (*9*) (Fig. 11). This is one of the longest observed lifetimes of any purely inorganic compound. Shifts in the near-UV absorption band upon variation of the Y ligands in $\{Mo_6Y_8\}^{4+}$ and $\{W_6Y_8\}^{4+}$ were initially taken as an indication that the transition originates from an (inner) ligand-to-metal charge transfer; however, the

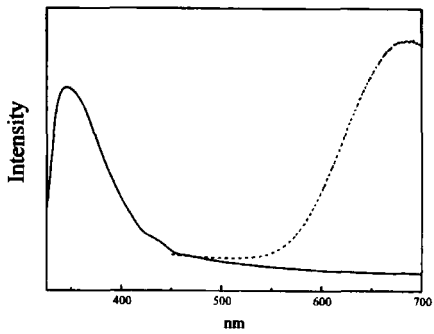

FIG. 11. Absorption (full) and emission (dashed) spectra of $[Bu_4N]_2[Mo_6Cl_8Cl_6]$ in CH_2Cl_2.

independence of the emission spectra of the $\{Mo_6X_8\}^{4+}$ unit on changing the identity of inner ligands suggests that the transition responsible for radiative decay is between purely metal-based orbitals (*10, 77, 85, 86*). The $\{W_6Y_8\}^{4+}$ clusters display emission spectra that vary only slightly with changes in the inner and outer ligands. A summary of the photophysical data for various molybdenum and tungsten clusters is given in Table II. The low rate constants for the red-shifted radiative decay are attributed to a spin- and symmetry-forbidden character of the transition. Also important to the low rate constants is the absence of high-energy vibrational modes capable of deactivating the excited state. Additionally, the halide ligands appear to shield the Mo_6 and W_6 core and thereby inhibit energy transfer to solvent molecules.

From the photophysical and electrochemical data on $[Mo_6Cl_8Cl_6]^{2-}$, a modified Latimer diagram can be constructed relating the excited cluster $[Mo_6Cl_8Cl_6]^{2-*}$ to the oxidized and reduced ground states (*74*) (Fig. 12). When $[Mo_6Cl_8Cl_6]^{2-*}$ is quenched with an electron donor such as benzoquinone, $[Mo_6Cl_8Cl_6]^{3-}$ is generated. Similarly, $[Mo_6Cl_8Cl_6]^{2-*}$ is quenched by the electron acceptor phenothiazine to produce $[Mo_6Cl_8Cl_6]^{1-}$. The long excited-state lifetime of $[Mo_6Cl_8Cl_6]^{2-*}$ and the strong reducing and oxidizing nature of the electronically

TABLE II

PHOTOPHYSICAL DATA[a] OF $\{M_6Y_8\}^{n+}$ CLUSTERS

Cluster	$\lambda_{max,em}$	τ (μs)	k_r (10^3 s^{-1})	k_{nr} (10^3 s^{-1})	Refs.
$[Mo_6Cl_8Cl_6]^{2-}$	805	180	1.1	4.5	*10, 85*
$[Mo_6Cl_8Br_6]^{2-}$		140			*89*
$[Mo_6Cl_8I_6]^{2-}$		86			*89*
$[Mo_6Br_8Cl_6]^{2-}$		190			*89*
$[Mo_6Br_8Br_6]^{2-}$	825	110	2.1	7.0	*10, 85*
$[Mo_6Br_8I_6]^{2-}$		71			*89*
$[Mo_6I_8I_6]^{2-}$		84	1.9	10	*85*
$[W_6Cl_8Cl_6]^{2-}$	880	2.2	13	650	*10, 77, 89*
$[W_6Cl_8Br_6]^{2-}$	814	4.4	10	490	*85, 89*
$[W_6Cl_8I_6]^{2-}$	802	5.6	23	310	*77, 89*
$[W_6Br_8Cl_6]^{2-}$	766	15	10	93	*77, 89*
$[W_6Br_8Br_6]^{2-}$	758	15	8	59	*77, 84*
$[W_6Br_8I_6]^{2-}$	752	19	17	50	*89*
$[W_6I_8Cl_6]^{2-}$	701	16	11	89	*77, 89*
$[W_6I_8Br_6]^{2-}$	698	27	11	34	*77, 89*
$[W_6I_8I_6]^{2-}$	698	30	13	20	*77, 84*

[a] Values are reported with acetonitrile solutions of cluster.

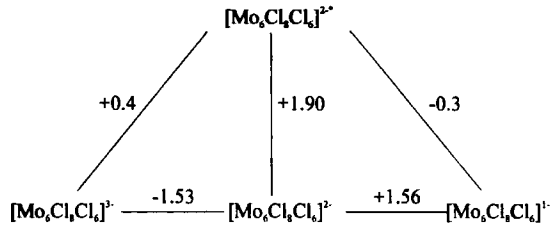

FIG. 12. Latimer diagram of $[Mo_6Cl_8Cl_6]^{2-}$. Excited state energy in eV; electrode potentials estimated vs. SCE in CH_3CN.

quenched clusters should be useful for converting solar energy to chemical energy (*73*).

The potentials in the excited-state Latimer diagram demonstrate that the annihilation reactions of $[Mo_6Cl_8Cl_6]^{3-}$ and $[Mo_6Cl_8Cl_6]^{1-}$ liberate enough energy to generate $[Mo_6Cl_8Cl_6]^{2-*}$ and electrogenerated chemiluminescence (ECL). This phenomenon has been used extensively to study electron transfer reactions between the excited states of a broad range of the halide clusters $[M_6X_8Y_6]^{2-}$ (M = Mo, W; X = Cl, Br, I; Y = Cl, Br, I) in combination with both electron donors and acceptors (*78*, *87*, *88*). Chemical oxidation of benzyl alcohol and 2-propanol by electrochemically generated $[Mo_6Cl_8Cl_6]^{1-}$ has been demonstrated; however, photochemically generated $[Mo_6Cl_8Cl_6]^{1-}$ is less effective for the oxidation of alcohols (*75*). The excited cluster $[Mo_6Cl_8Cl_6]^{2-*}$ is quenched by molecular oxygen through an energy transfer mechanism to generate singlet oxygen, which was identified by reaction with 1-methylcyclohexene (*89*).

E. Molecular and Electronic Structure of the Group 6 Metal Halide Clusters

1. Electronic Structure

Electronic structure calculations carried out at a variety of levels on these octahedral metal-halide clusters vary in detail (*90–104*). Our view of the metal-based orbitals responsible for metal–metal bonding in the $\{M_6Y_8\}^{4+}$ unit has evolved very little since Cotton and Haas' semiempirical treatment in 1964 (*90*). Undoubtedly the importance of symmetry in the calculations has led to the consistent description of the bonding scheme. Only a brief summary emphasizing the relation between the proposed models to the physical and chemical properties of the clusters is presented here. For a more detailed discussion of the bonding numerous reviews are available (*105–109*).

Orbitals responsible for the metal–metal bonding in $\{M_6Y_8\}^{4+}$ have a_{1g}, t_{1u}, t_{2g}, t_{2u}, and e_g symmetry and are directed along the edges of the M_6 framework, generating 12 two-electron bonds. A total of 24 cluster bonding electrons, CBE (CBE number is equal to the number of valence electrons of the metal atoms minus the number of anionic ligands and the charge of the cluster) fill the bonding orbitals, creating "closed shell" diamagnetic compounds (Fig. 13). ESR measurements are consistent with the proposed diamagnetism of $[M_6Y_8X_6]^{2-}$ (M = Mo, W) clusters and paramagnetism of the oxidized species $[M_6Y_8X_6]^{1-}$ (*10*, *79*).

Some dispute persists as to the size of the highest occupied molecular orbital (HOMO)–lowest unoccupied molecular orbital (LUMO) gap in the closed-shell 24-electron species. This aspect of the molecular orbital diagram is of particular interest for its implications on the photophysical properties of the clusters. Electrochemical measurements are consistent with a large, 2- to 3-eV, separation; however, the exact nature of the excited state remains uncertain.

2. *Molecular Structure*

These highly symmetric compounds provide aesthetically pleasing structures with near perfect Mo_6 and W_6 octahedrons that expand and contract to accommodate different coordination environments. Comprehensive studies of the structures of the halide clusters $[Mo_6Y_8X_6]^{2-}$

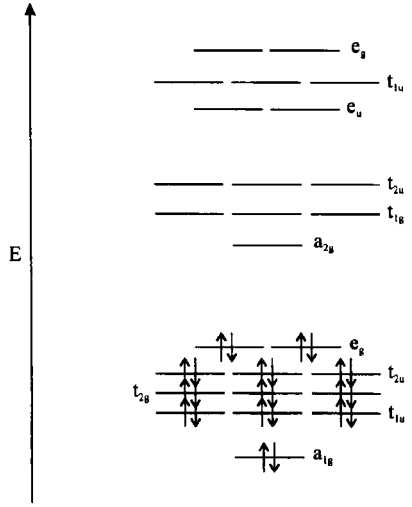

FIG. 13. A molecular orbital diagram for $\{M_6Y_8\}^{4+}$ based on an Extended Hückel calculation, adapted from reference (*108*).

(Y = Cl, Br, I; X = F, Cl, Br, I) by Preetz reveals that both electronic and steric effects of the inner and outer ligands influence the Mo–Mo, Mo–Y, and Mo–X bond lengths (*42*, *43*, *110*). For a given $\{Mo_6Y_8\}^{4+}$ (Y = Cl, Br, I) core, the Mo–Mo bond length increases with the axial ligands series X = F < Cl < Br < I (Table III). Expansion of the Mo_6 octahedron is attributed to changes in the electronegativity of the axial ligands. The ^{95}Mo NMR spectra of the various halide clusters reveal that resonances occur at the lowest field for complexes having six axial fluoride ligands. A high field shift occurs with increasing polarizability of the axial ligands, indicating that the electron density on the metal centers increases with decreasing electronegativity of the outer ligands. Because this increased electron density coincides with an expansion of the Mo_6 octahedron, it is reasonable to assume that the added electron density increases occupation of the antibonding orbitals of the Mo_6 framework. In addition to increasing the electron density on the metal centers, changes in the identity of the axial ligands X from F to I also result in a reduced HOMO–LUMO gap as the ligand field strength of X decreases. The ^{95}Mo NMR shift of the halide clusters varies linearly with the electronegativity of the axial ligands (*110*), and a similar relationship exists between the ^{95}Mo NMR shift and the Mo–Mo bond length (Fig. 14).

TABLE III

SELECTED BOND LENGTHS[a] OF SOME $[Mo_6Y_8X_6]^{2-}$ CLUSTERS

Cluster	d(Mo–Mo)	d(Mo–Y)	d(Mo–X)	d(Y–Y)	d(Y–X)	Ref.
$[Mo_6Cl_8F_6]^{2-}$	2.593	2.488	1.993	3.517	3.234	*42*
$[Mo_6Cl_8Cl_6]^{2-}$	2.602	2.469	2.420	3.489	3.523	*42*
$[Mo_6Cl_8Br_6]^{2-}$	2.604	2.465	2.565	3.483	3.629	*42*
$[Mo_6Cl_8I_6]^{2-}$	2.615	2.466	2.788	3.484	3.801	*42*
$[Mo_6Br_8F_6]^{2-}$	2.618	2.622	2.012	3.710	3.305	*43*
$[Mo_6Br_8Cl_6]^{2-}$	2.636	2.604	2.451	3.680	3.591	*43*
$[Mo_6Br_8Br_6]^{2-}$	2.640	2.600	2.491	3.674	3.675	*43*
$[Mo_6Br_8I_6]^{2-}$	2.644	2.598	2.815	3.673	3.854	*43*
$[Mo_6I_8F_6]^{2-}$	2.650	2.798	2.008	4.006	3.394	*110*
$[Mo_6I_8Cl_6]^{2-}$	2.655	2.775	2.460	3.923	3.656	*43*
$[Mo_6I_8Br_6]^{2-}$	2.670	2.775	2.616	3.924	3.764	*43*
$[Mo_6I_8I_6]^{2-}$	2.675	2.767	2.846	3.911	3.923	*43*
$[Mo_6(Cl_7S)Cl_6]^{3-}$	2.609	2.479[b]	2.468			*66*
$[Mo_6(Cl_7Se)Cl_6]^{3-}$	2.616	2.501[b]	2.471			*66*
$[Mo_6(Cl_6Se_2)Cl_6]^{4-}$	2.610	2.513[b]	2.496	3.559	3.591	*67*

[a] All distances are in Å.

[b] Chalcogens are disordered over the capping positions.

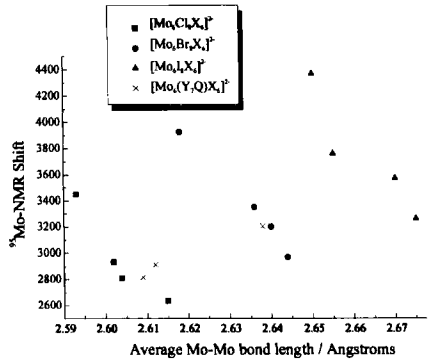

FIG. 14. Plot of ^{95}Mo NMR shift vs. average Mo–Mo bond length. Data are taken from references (*43*, *66*).

The expansion of the Mo_6 octahedron correlates with contraction of the cubic array of the eight inner ligands and shortening of the Mo–Y bonds. The net result of these distortions is a deviation in the planarity of the Mo–Y_4 units on the face of the Y_8 cube (Fig. 15). The Mo atoms of the clusters $[Mo_6Cl_8X_6]^{2-}$ (X = F, Cl, Br, I) protrude outside the halide cube with progressively increasing distances as the axial ligand is changed from F through I. At the other extreme, the metal atoms lie within the I_8 cube and approach the Y_4 face as X increases in size for $[Mo_6I_8X_6]^{2-}$. The $[Mo_6Br_8X_6]^{2-}$ clusters exhibit intermediate structures, with the metal atoms of $[Mo_6Br_8F_6]^{2-}$ inside the halide cube and those of $[Mo_6Br_8Br_6]^{2-}$ and $[Mo_6Br_8I_6]^{2-}$ outside. With the exception of $[Mo_6Cl_8F_6]^{2-}$ and $[Mo_6Br_8F_6]^{2-}$, overlap of the inner and outer ligands induces a strain within the cluster framework, and this strain becomes more pronounced as the size of either X or Y increases. The strain may account for the increased reactivity in clusters with larger ligands (*26*, *27*).

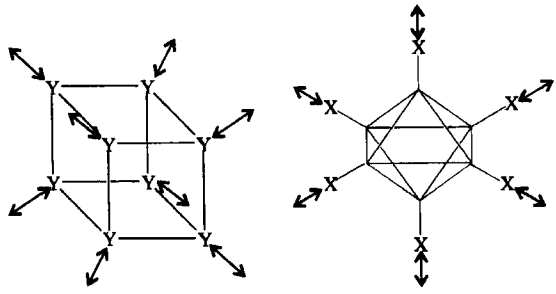

FIG. 15. Distortions of Y_8 cube and X_6 octahedron with changes in X or Y.

Changes in the inner ligands Y of the clusters $[M_6Y_8X_6]^{2-}$ from Cl to I results in an expanded M_6 octahedron and a Y_8 cube. Substitution of chalcogenide atoms for the inner halide ligands has only a modest effect on the average Mo–Y and Mo–Mo bond length (Table III), with the chalcogenide ligands distributed among two or more face-capping sites. However, the terminal chloride–molybdenum bond lengths are elongated compared to the all-halide clusters. These bond length changes have been attributed to decreased electrostatic attraction between the axial chloride ligands and the less positive halide–chalcogenide cores $\{Mo_6Y_{8-z}Q_z\}^{(4-z)+}$.

The pseudo-halide derivatives $[Mo_6X_8Y_6]^{2-}$ (X = Cl, Br; Y = N_3 (*46*), NCO (*47*), NCS (X = Cl only) (*40*, *111*, *112*), and NCSe (*47*)) have been reported and crystallographically characterized. Some discrepancies exist in the assignment of the disposition of the ambidentate ligands. For instance, both N- and O-bound cyanate are indicated by ^{14}N NMR in tetrachloroethane; however, crystallographic studies are consistent with N-bound cyanate ligands. Selenocyanate is found to be exclusively N-bound by ^{14}N NMR, IR, and X-ray crystallography. Thiocyanate ligands of most $[Mo_6Cl_8(SCN)_6]^{2-}$ salts are assigned as N-bound to the cluster, with the exception of $K_2[Mo_6Cl_8(SCN)_6]$, which has been identified as S-bound in both the solid state and solution. Interestingly, structures of the cluster anions $[Mo_6Br_8(N_3)_6]^{2-}$ vary with the type of counterion, including relatively noninteracting $[Bu_4N]^+$ and $[Ph_3P{=}N{=}PPh_3]^+$. The cluster anions of these salts have regular octahedral geometries; however, the Mo–Mo and Mo–Br bonds vary by as much as 8% between the two structures.

Several vibrational studies of the $[M_6Y_8X_6]^{2-}$ clusters have been reported (*12*, *53*, *113–117*). The structures of these compounds led Hogue and McCarley to predict that extensive mixing of the symmetry coordinates in the normal modes would prevent the application of group-frequency concepts (*12*); however, diagnostic M–M, M–X, M–Y, and X–M–Y stretching frequencies have been identified, and they find use in the characterization of the clusters. Selection rules for the high-symmetry (O_h) halide clusters $[M_6Y_8X_6]^{2-}$ (Y = Cl, Br, I; X = F, Cl, Br, I) predict a total of ten Raman active ($3A_{1g} + 3E_g + 4T_{2g}$) and five IR ($5T_{1u}$) active modes. The three totally symmetric (A_{1g}) bands, which consist of the breathing mode of the M_6 octahedron, the Y_8 cube, and the terminal X_6 ligands, are virtually unmixed and thus provide diagnostic features that are easily identified by their totally polarized Raman bands. Decreased symmetry in the environment about the M_6 core, owing to site symmetry in the solid or the presence of axial ligands having lower symmetry, does not prevent application of group-frequency concepts.

Pyridine *N*-oxide derivatives, $Mo_6Cl_8Cl_4(ONC_5H_4R)_2$, have been prepared, and the ν(Mo–O) band was assigned around 1200–1270 cm^{-1}. The ν(M–O) frequencies correlated with the Hammett constant σ of the R group. As the R group becomes more electron withdrawing (or increases in σ), the ν(Mo–O) stretching frequency decreases. This observation contrasts with trends in the ν(M–O) frequency with late-transition metal complexes such as Ni, Co, and Cu, in which the M–O vibrational energy increases with the electron-withdrawing nature of the R group and indicates that π-bonding is unimportant in the axial ligand–metal bonds (*31*).

Oxidation of the $\{M_6Y_8\}^{4+}$ core removes electrons from the bonding orbitals of the M_6 framework, causing an expansion of the metal octahedron. Few of these oxidized clusters have been isolated and structurally characterized. The EPR spectrum of $[Mo_6Cl_8Cl_6]^{1-}$ indicates that the compound is distorted along one axis; however, single-crystal X-ray data is not available to confirm this distortion. The EPR spectrum of the oxidized tungsten cluster $[W_6Br_8Br_6]^{1-}$ contrasts with the spectrum of $[Mo_6Cl_8Cl_6]^{1-}$ in that the values are consistent with an undistorted octahedron, which has been verified by the crystal structure of $[(Ph_3P)_2N][W_6Br_8Br_6]$ (*10*, *79*).

III. Group 5 Metal Halide Clusters

Clusters containing the $\{Ta_6Cl_{12}\}^{2+}$ and $\{Nb_6Cl_{12}\}^{2+}$ cores have been known for nearly as long as those of the group 6 metals, and their structures were first reported by Linus Pauling (*118*). Despite the long history of the group 5 metal halide clusters $\{M_6Y_{12}\}^{n+}$ (M = Nb, Ta) the ligand substitution chemistry is not as well developed as that of the analogous group 6 metal compounds $\{M_6Y_8\}^{4+}$ (M = Mo, W), because of the extensive redox chemistry associated with the $\{M_6Y_{12}\}^{n+}$ core. Five different oxidation states have been observed for the Nb and Ta cores, with compounds in the n = 2–4 states being most common. The n = 1 and n = 5 states are electrochemically accessible; however, clusters in these oxidation states have not been isolated. As the average oxidation state changes for the metals in the cluster core $\{M_6Y_{12}\}^{n+}$, the affinity for the axial ligands is altered. In the more electron-rich (reduced) state, the clusters have higher affinity for π-acid ligands such as phosphines, and in the more electron-deficient state, the core has a greater affinity for π-donor ligands such as chloride. Thus, the stability of a particular oxidation state is altered by the coordination environment about the $\{M_6Y_{12}\}^{n+}$ core.

A. Synthesis of Cluster Core

The most convenient route to $\{M_6Y_{12}\}^{2+}$ clusters of niobium and tantalum is the conproportionation of the pentahalides NbY_5 and TaY_5 (Y = Cl, Br) with excess of the metal in molten alkali halide:

$$20NaY + 14MY_5 + 16M \rightarrow 5Na_4M_6Y_{18}. \quad (13)$$

Formation of lower nuclearity compounds can be avoided by using a 10 to 7 ratio of NaY to MY_5 (*119*). The conproportionation reaction is convenient for the synthesis of the group 5 metal clusters because it allows the use of glass reaction vessels as opposed to electron-beam-sealed metal tubes, it provides almost quantitative yield of cluster (in excess of 90%), and it requires only 24 h for the reaction to reach completion, as opposed to 4–6 days. Work-up of the product in aqueous acid HY solutions with small amounts of stannous chloride to prevent oxidation produces $M_6Y_{14}\cdot 8H_2O$. Unlike the group 6 polymeric materials M_6Y_{12}, $M_6Y_{14}\cdot 8H_2O$ consists of discrete molecules with a $\{M_6Y_{12}\}^{+}$ core coordinated by two halide ligands and four water molecules, and is accurately described as $M_6H_{12}Y_2(H_2O)_4\cdot 4H_2O$. The soluble tertiary salts $A_4Nb_6Y_{12}Y_6$ have been used as precursors to other cluster compounds with the $\{Nb_6Y_{12}\}^{2+}$ core, with limited success (*120*, *121*).

B. Redox Chemistry of the Group 5 Clusters

Initial studies on the redox properties of the $\{M_6Y_{12}\}^{n+}$ clusters were reported on poorly defined complexes simply noted as $[Ta_6Cl_{12}]^{2+}$ or $[Nb_6Cl_{12}]^{2+}$ (*122*). Aqueous cluster solutions were prepared from the sulfate salts $Ta_6Cl_{12}SO_4$ and $Nb_6Cl_{12}SO_4$ with various electrolytes. Some combination of water molecules and anions fills the coordination sphere of the $\{M_6Y_{12}\}^{n+}$ cluster. Despite these ambiguities, the oxidized compounds $\{M_6Y_{12}\}^{4+}$ were obtained with various chemical oxidants by a two-electron transfer process (*123*):

$$\{M_6Y_{12}\}^{2+} + 2Ox \rightarrow \{M_6Y_{12}\}^{4+} + 2Red. \quad (14)$$

Subsequent investigations (*124–126*) revealed an equilibrium between the intermediate $\{M_6Y_{12}\}^{3+}$ state and the $\{M_6Y_{12}\}^{2+}$ and $\{M_6Y_{12}\}^{4+}$ clusters,

$$2\{M_6Y_{12}\}^{3+} \rightleftharpoons \{M_6Y_{12}\}^{2+} + \{M_6Y_{12}\}^{4+} \quad (15)$$

and a slow disproportionation of the oxidized $\{Ta_6Y_{12}\}^{4+}$ (Y = Cl, Br) cluster to mononuclear Ta(V) complexes and the reduced clusters $\{Ta_6Y_{12}\}^{2+}$ and $\{Ta_6Y_{12}\}^{3+}$.

Cyclic voltammetry studies (*127*) on $\{Ta_6Br_{12}\}^{2+}$ reveal two reversible one-electron oxidations corresponding to generation of the $n = 3$ and $n = 4$ states,

$$\{Ta_6Br_{12}\}^{2+} \underset{+e}{\overset{-e}{\rightleftharpoons}} \{Ta_6Br_{12}\}^{3+} \underset{+e}{\overset{-e}{\rightleftharpoons}} \{Ta_6Br_{12}\}^{4+}, \tag{16}$$

suggesting only a minimal structural rearrangement upon changing oxidation state. Contrasting results were obtained by Hussey and coworkers (*128*, *129*) who investigated the cyclic voltammetry response of $[Ta_6Cl_{12}Cl_6]^{(6-n)-}$ in acetonitrile. Three 1-electron transfer processes were observed, corresponding to generation of the $n = 2$–5 species. The reduced cluster $[Ta_6Cl_{12}Cl_6]^{4-}$ undergoes facile substitution by an acetonitrile molecule, generating $[Ta_6Cl_{12}Cl_5(CH_3CN)]^{3-}$ (Fig. 16), which is detected in the voltammogram along with the liberated chloride ion. Noncoordinating electrolytes in methylene chloride prevent the loss of the chloride ligand, and the redox couples are chemically reversible (Fig. 16). Interestingly, $[Ta_6Cl_{15}(OSO_2CF_3)_6]^{2-}$ undergoes two reversible one-electron reductions in acetonitrile to generate $[Ta_6Cl_{12}(OSO_2CF_3)_6]^{3-}$ and $[Ta_6Cl_{12}(OSO_2CF_3)_6]^{4-}$, with no evidence for

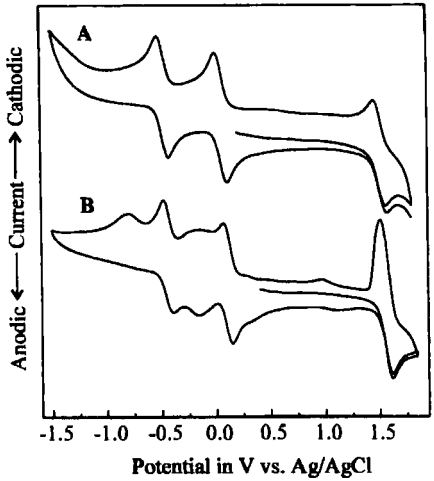

FIG. 16. Cyclic voltammogram of $[Bu_4N]_3[Ta_6Cl_{12}Cl_6]$ in **(A)** CH_2Cl_2 and **(B)** CH_3CN 0.1 M $[Bu_4N]BF_4$. Sweep rate is 0.10 V/s.

ligand displacement on the cyclic voltammetry time scale. Presumably the strong σ- and π-donor properties of the chloride ions weaken the Ta–Cl^a bonds of $[Ta_6Cl_{12}Cl_6]^{4-}$, making the chloride ligands susceptible to displacement. In contrast, the reduced $\{Ta_6Cl_{12}\}^{2+}$ core of $[Ta_6Cl_{12}(OSO_2CF_3)_6]^{4-}$ is stabilized by the weak donor properties of the triflate ligands.

In acidic chloroaluminate melts, the redox potentials of the $\{Ta_6Cl_{12}\}^{2+/3+}$ and $\{Ta_6Cl_{12}\}^{3+/4+}$ couples are anodically shifted by one volt compared to values obtained in acetonitrile electrolytes, suggesting that the majority of the axial chloride ligands have been replaced by $[AlCl_4]^-$ ions (*129*). A similar shift in the redox potentials of the $\{Nb_6Cl_{12}\}^{2+/3+}$ and $\{Nb_6Cl_{12}\}^{3+/4+}$ couples is observed when changing from a basic chloroaluminate melt to an acidic one. In Cl^--rich molten salts, the highly reduced cluster $[Nb_6Cl_{12}Cl_6]^{5-}$ with a $\{Nb_6Cl_{12}\}^{1+}$ core is accessible (*128*), but this species is not accessible in acidic melts or acetonitrile (*130*). At the other extreme, the highly oxidized cluster $[Nb_6Cl_{12}Cl_6]^{1-}$ with a $\{Nb_6Cl_{12}\}^{5+}$ core is generated at 1.76 V vs. SCE in acetonitrile electrolytes.

C. Ligand Substitution

The ligand substitution chemistry of the $[Nb_6Y_{12}X_6]^{(6-n)-}$ and $[Ta_6Y_{12}X_6]^{(6-n)-}$ clusters is complicated by disproportionation reactions and dependence of the ligand affinity on the oxidation state of the cluster. Unless measures are taken to control chemical potentials, unwanted redox reactions can produce mixtures of partially substituted clusters in a mixture of oxidation states. Consequently, no strategies for exchanging all six axial ligands with a wide range of donor groups exist. Instead, a number of less versatile methods have been developed that introduce a limited range of ligands at the axial positions and provide moderate control of the redox chemistry.

The axial ligands of $A_4Nb_6Y_{12}Y_6$ (A = alkali metal; Y = Cl, Br) undergo simple metathesis with azide and thiocyanate. Dissolution of $A_4Nb_6Y_{12}Y_6$ in alcohol solutions of N_3^- or NCS^- produces the crystalline compounds $A_4Nb_6Y_{12}X_6$ (X = N_3, NCS) (*131–133*). Long reaction times, on the order of weeks, are required when the $A_4Nb_6Y_{12}Y_6$ clusters are used as precursors to new cluster compounds. Also, the relative affinity of the $\{M_6Y_{12}\}^{2+}$ core for different anionic and neutral ligands is unknown and may restrict the types of clusters accessible from $A_4Nb_6Y_{12}Y_6$.

The hydrated complexes $M_6Y_{12}Y_2(H_2O)_4 \cdot 4H_2O$ (M_6Y_{14}) provide more versatile precursors to new $\{M_6Y_{12}\}^{2+}$ (M = Nb, Ta) derivatives. The

aqua ligands are slowly displaced by neutral L or anionic X^- donor ligands, generating $M_6Y_{12}Y_2L_4$ or $[M_6Y_{12}Y_2X_4]^{4-}$ (*31*, *134–136*). The range of ligands amenable to this strategy has not been delineated, but if care is taken to prevent oxidation of the cluster, a variety of π-acids are likely to bind to the reduced $\{M_6Y_{12}\}^{2+}$ core. Saito and coworkers used chromatography to isolate the *cis* and *trans* isomers of the phosphine complexes $[M_6Cl_{12}Cl_2(PR_3)_4]$ in moderate yields (13–37%) (*135*) (Fig. 17). Also isolated in the separation procedure was the trisubstituted cluster $[Ta_6Cl_{12}Cl_3(PEt_3)_3]$, indicating that substitution of the water molecules of $Ta_6Cl_{12}Cl_2(H_2O)_4 \cdot 4H_2O$ is more complex than first proposed.

Repeated addition of aliphatic alcohols ROH to $M_6Y_{12}Y_2(H_2O)_4 \cdot 4H_2O$ (M = Nb, Ta; Y = Cl, Br) under an oxygen-free atmosphere eventually yields $[M_6Y_{12}(ROH)_6]X_2$ (*137*). Interestingly, ^1H NMR and conductivity measurements indicate that the axial halide ligands (especially bromide) are displaced by methanol before the axial water ligands (*138*). Under anaerobic conditions $[M_6Y_{12}(OCH_3)_2(HOCH_2)_4]$ can be obtained from methanolic solutions of $M_6Y_{12}Y_2(H_2O)_4 \cdot 4H_2O$ and two equivalents of sodium methoxide (*139*). Care must be taken to exclude air from these reaction mixtures to avoid unwanted oxidation of the cluster.

In basic solutions the $\{M_6Y_{12}\}^{2+}$ core is rapidly oxidized upon exposure to air. Presumably the strong σ- and π-donor properties of hydroxide and alkoxide ligands increase electron density on the

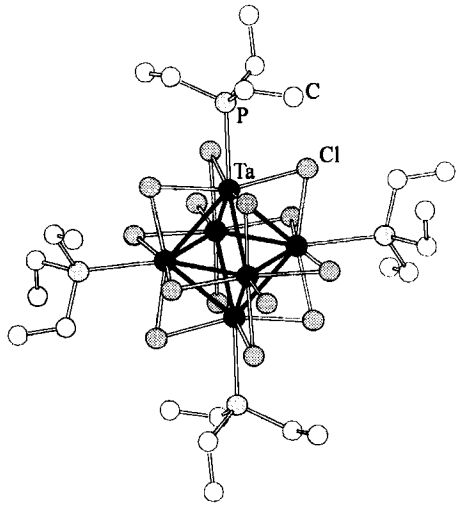

FIG. 17. Structure of *trans*-$Ta_6Cl_{12}Cl_2[P(C_2H_5)_3]_4$.

$\{M_6Y_{12}\}^{2+}$ core, making the clusters $[M_6Y_{12}(OR)_6]^4$ (R = H, CH_3) susceptible to oxidation. Titration of $M_6Y_{12}Y_2(H_2O)_4$ with OH^- precipitates the neutral complex $M_6Y_{12}(OH)_2(H_2O)_4 \cdot 6H_2O$ under N_2 (*140*). Isolation of $M_6Y_{12}(OH)_2(H_2O)_4 \cdot 6H_2O$ indicates that the axial chloride ligands are displaced in preference to the axial H_2O ligands. Subsequent addition of OH^- yields $A_4M_6Y_{12}(OH)_6$. In oxygen-containing atmospheres, $M_6Y_{12}(OH)_4(H_2O)_2$ precipitates and then redissolves as $A_2M_6Y_{12}(OH)_6$ with increasing pH (*141*). The methoxide clusters $M_6Y_{12}(OCH_3)_2(HOCH_3)_4$ and $A_2M_6Y_{12}(OCH_3)_6$ have been prepared in a similar fashion (*139*) (Fig. 18).

In acid environments the $\{M_6Y_{12}\}^{2+}$ core of $M_6Y_{12}Y_2(H_2O)_4 \cdot 4H_2O$ is oxidized to either $\{M_6Y_{12}\}^{3+}$ or $\{M_6Y_{12}\}^{4+}$ depending on the metal, inner ligand, and acid source. Hydrochloric acid oxidizes $Ta_6Cl_{12}Cl_2(H_2O)_4$ to $Ta_6Cl_{12}Cl_4(H_2O)_2$ with a $\{Ta_6Cl_{12}\}^{4+}$ core (*142*); however, $Nb_6Cl_{12}Cl_2(H_2O)_4$ is oxidized to $[Nb_6Cl_{12}Cl_6]^{3-}$ with a $\{Nb_6Cl_{12}\}^{3+}$ core (*143*, *144*). Synthesis of the two-electron oxidized cluster $[Nb_6Cl_{12}Cl_6]^{2-}$ requires chlorine gas to oxidize $Nb_6Cl_{12}Cl_2(H_2O)_4$ (*143*, *145*).

Introduction of the weakly coordinating triflate ion at the axial positions of the $\{M_6Y_{12}\}^{n+}$ cluster is accomplished by the reactions

$$[Bu_4N]_2[Ta_6Cl_{12}Cl_6] + x\text{sHOSO}_2CF_3 \rightarrow [Bu_4N]_2[Ta_6Cl_{12}(OSO_2CF_3)_6] + 6HCl(g). \quad (17)$$

The resulting cluster is an electron deficient species (*146*) (Fig. 19). The niobium analog $[Bu_4N]_3[Nb_6Cl_{12}(OSO_2CF_3)_6]$ has also been prepared. Cyclic voltammetry on solutions of $[Bu_4N]_2[Ta_6Cl_{12}(OSO_2CF_3)_6]$ reveals two 1-electron transfers at 0.89 V and 0.29 V vs. Ag/AgCl, corresponding to generation of $[Ta_6Cl_{12}(OSO_2CF_3)_6]^{3-}$ and $[Ta_6Cl_{12}(OSO_2CF_3)_6]^{4-}$, respectively. These reduction potentials are among the

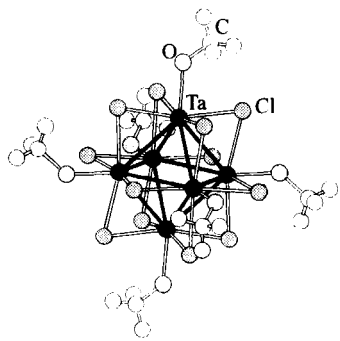

FIG. 18. Structure of $[Ta_6Cl_{12}(OCH_3)_6]^{2-}$.

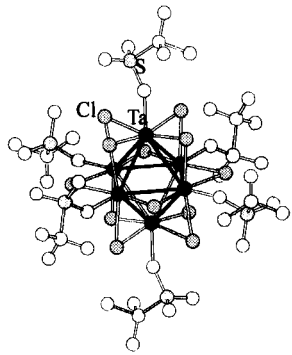

FIG. 19. Structure of $[Ta_6Cl_{12}(OSO_2CF_3)_6]^{2-}$.

most positive observed for the $\{Ta_6Cl_{12}\}^{4+}$ and $\{Ta_6Cl_{12}\}^{3+}$ clusters and attest to the poor donor strength of the triflate ion. The strong oxidizing character of $[Bu_4N]_2[Ta_6Cl_{12}(OSO_2CF_3)_6]$ prevents the simple metathesis reactions with anionic ligands X^- such as Cl^-, Br^-, I^-, NCS^-, and CN^- that are observed with the analogous $[Bu_4N]_2[Mo_6Cl_8(OSO_2CF_3)_6]$ (*40*). Instead, a complex redox process accompanies the substitution reactions and reduced clusters $[Bu_4N]_3[Ta_6Cl_{12}X_6]$ (X = Cl, Br, I, NCS) are obtained. A slight excess of X^- is required for complete substitution of the triflate ligands, and the reaction rate increases with the ligand series $Cl^- < Br^- < NCS^- < I^- < CN^-$. This trend does not follow the basicity or polarizability of the ligand, so other factors, possibly oxidation potentials of X^-, influence the redox/substitution process. In fact the reduced cluster $[Ta_6Cl_{12}(OSO_2CF_3)_6]^{3-}$ is observed spectroscopically as an intermediate. Reduction of $[Ta_6Cl_{12}(OSO_2CF_3)_6]^{2-}$ by Cl^- (1.29 V vs. Ag/AgCl) would not be predicted from redox potentials; however, refluxing methylene chloride solutions of $[Bu_4N]_2[Ta_6Cl_{12}(OSO_2CF_3)_6]$ and $[Bu_4N]Cl$ yields the reduced product $[Bu_4N]_3[Ta_6Cl_{12}Cl_6]$. It is likely that oxidation of Cl^- is promoted by loss of Cl_2 due to a slow stream of N_2 passed over the reaction mixture. In mixtures of $[Bu_4N]_2[Ta_6Cl_{12}(OSO_2CF_3)_6]$ and the more reducing ligands I^-, Br^-, and NCS^-, the reduced cluster core $\{Ta_6Cl_{12}\}^{2+}$ is detected spectroscopically and the proposed reaction/substitution scheme in Fig. 20 is proposed. Surprisingly, the simple metathesis reaction

$$[Ta_6Cl_{12}(OSO_2CF_3)_6]^{2-} + xsX^- \text{ (or L)} \rightarrow [Ta_6Cl_{12}X_6]^{2-} \text{ (or } [Ta_6Cl_{12}L_6]^{4+}) + 6\ OSO_2CF_3^- \quad (18)$$

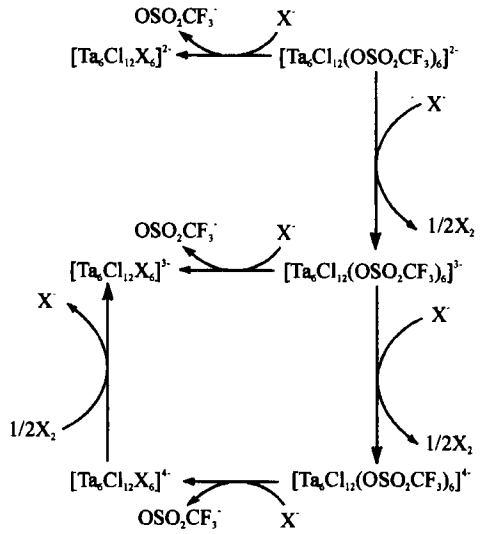

FIG. 20. Reaction scheme of $[Ta_6Cl_{12}(OSO_2CF_3)_6]^{2-}$ with X^-.

is not observed for any anionic, X^-, or neutral, L, ligands including phosphine oxides.

D. Electronic and Molecular Structure

Numerous electronic structure calculations on the $\{M_6Y_{12}\}^{n+}$ cluster have been performed at various levels (*90*, *91*, *93*, *94*, *96*, *98*, *104*). The molecular orbital structure obtained from extended Hückel calculations indicates that the eight metal-based orbitals responsible for M–M bonding in the $\{M_6Y_{12}\}^{n+}$ unit have a_{1g}, t_{2g}, t_{1u}, and a_{2u} symmetry (*147*) (Fig. 21). In contrast to the directionality of the bonding orbitals in $\{M_6Y_8\}^{4+}$ (see Section II.E.1), the bonding orbitals of $\{M_6Y_{12}\}^{n+}$ are directed along the faces of the metal octahedron, creating 8 three-center, two-electron bonds. The number of cluster-bonding electrons available to fill the eight bonding orbitals is equal to the number of valence electrons of the metals minus the number of anionic ligands and the charge of the cluster. Thus, $[Nb_6Cl_{12}Cl_6]^{4-}$ is electron precise, with 16 CBE [30 − 18 − (−4)], and $[Nb_6Cl_{12}Cl_6]^{4-}$ is electron deficient with 14 CBE.

The exact bonding or antibonding character of the a_{2u} level differs among the various calculations depending on how the contribution of the axial ligands to the molecular orbitals is considered. Oxidation of the $\{Nb_6Cl_{12}\}^{2+}$ core to $\{Nb_6Cl_{12}\}^{4+}$ corresponds to depopulation of the

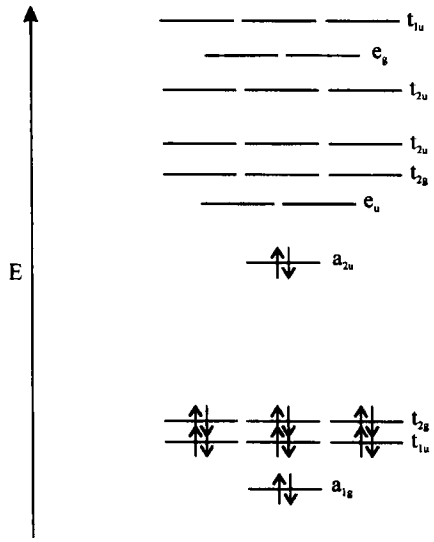

FIG. 21. A molecular orbital diagram for $\{M_6Y_{12}\}^{n+}$ based on an extended Hückel calculation, adapted from reference (*108*).

a_{2u} level; thus, the a_{2u} level is the HOMO or LUMO of the $n = 2$ or $n = 4$ clusters respectively. Magnetic susceptibility measurements and ESR spectra of the clusters with $n = 2$–4 confirm the assigned a_{2u} symmetry of the HOMO/LUMO (*148*). Hyperfine splitting of the unpaired electron of $[Nb_6Y_{12}X_6]^{3-}$ delocalized over the six niobium centers (spin 9/2) leads to impressively split ESR spectra (Fig. 22). X-ray

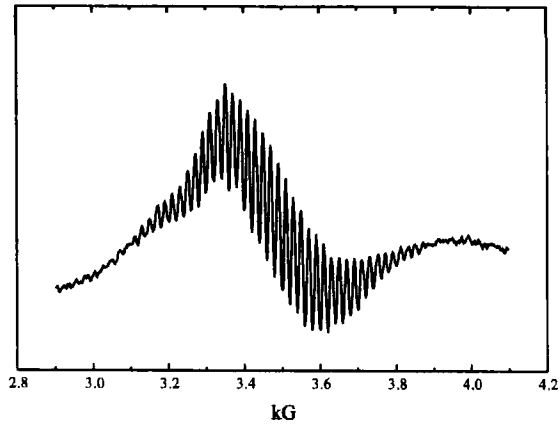

FIG. 22. EPR spectrum of $[Bu_4N]_3[Nb_6Cl_{12}Br_6]$ in CH_2Cl_2 at room temperature.

crystal structure determinations for the cluster series $[Nb_6Cl_{12}Cl_6]^{(n-6)-}$ reveal that the average Nb–Nb bond length decreases from 3.029 to 2.899 Å as the oxidation state on the $\{Nb_6Cl_{12}\}^{n+}$ core is lowered from $n = 4$ to $n = 2$ (*149*). This trend is consistent with the assignment of the a_{2u} level as predominately bonding in character for the all-chloro clusters. The high energy of the a_{2u} orbital explains the relative stability of the oxidized clusters $\{M_6Y_{12}\}^{3+}$ and $\{M_6Y_{12}\}^{4+}$. The average oxidation state of the metal atoms ranges from 2.33 ($n = 2$) to 2.66 ($n = 4$).

Numerous UV–vis absorption studies on the Nb and Ta clusters have been reported; however, despite the existence of one-to-one correspondence in the spectra of the two metals, there is little agreement on the assignments for the metal-based transitions (*135*, *150–152*). Solutions of both $\{Ta_6Y_{12}\}^{4+}$ and $\{Ta_6Y_{12}\}^{3+}$ are orange-brown in color, and the niobium analogs $\{Nb_6Y_{12}\}^{4+}$ and $\{Nb_6Y_{12}\}^{3+}$ are yellow-brown in solution. The reduced states $\{Nb_6Y_{12}\}^{2+}$ and $\{Ta_6Y_{12}\}^{2+}$ are olive green and green, respectively. Attempts to assign the electronic transitions of the clusters have been complicated by the similarity in the spectra of $\{M_6Y_{12}\}^{3+}$ and $\{M_6Y_{12}\}^{4+}$ clusters, which makes identifying mixtures of clusters in these oxidation states difficult. Additionally the $\{M_6Y_{12}\}^{2+}$ state is intensely colored and therefore easily obscures the spectra of the oxidized clusters.

E. Niobium Iodide Clusters $\{Nb_6I_8\}^{n+}$

Hexanuclear niobium iodide clusters $\{Nb_6I_8\}^{n+}$ are the lone exception to the usual edge-bridging halide geometry adopted by the group 5 metal halide clusters. With eight face-capping iodide ligands, the $\{Nb_6I_8\}^{n+}$ core is isostructural with the group 6 metal halide clusters $\{Mo_6Cl_8\}^{4+}$ and $\{W_6Cl_8\}^{4+}$ (*153*). The similarity in the metal-ligand configurations permits the use of the molecular orbital structure derived for the group 6 metal halides $\{M_6Y_8\}^{n+}$ to be applied to the $\{Nb_6I_8\}^{n+}$ unit. The $Nb_6I_8I_3$ is extremely electron deficient, with 19 CBE available for 12 metal–metal bonding orbitals. This unique electronic structure gives rise to the distinctive chemical and physical properties of $\{Nb_6I_8\}^{n+}$.

The binary phase $Nb_6I_8I_3$ is prepared (*154*) from the decomposition of Nb_3I_8 at 950°C:

$$13Nb_3I_8 \rightarrow 4Nb_6I_8I_3 + 15NbI_4. \qquad (19)$$

Increased yields are obtained when Niobium metal is added to the reaction mixture to reduce the NbI_4 by-product:

$$11NbI_4 + 13Nb \rightarrow 4Nb_6I_8I_3. \quad (20)$$

The addition of CsI to the reaction mixture produces the reduced cluster $CsNb_6I_8I_3$, with 20 CBE (*155*).

The electron deficiency of $Nb_6I_8I_3$ and $CsNb_6I_8I_3$ allows these compounds to absorb hydrogen in the solid state at 300°C and atmospheric pressure, generating $HNb_6I_8I_3$ and $CsHNb_6I_8I_3$ (*155*, *156*). Low-temperature neutron diffraction studies on $Nb_6I_8I_3$, $HNb_6I_8I_3$, and $DNb_6I_8I_3$ reveal that the hydrogen atom is slightly displaced from the center of gravity of the surrounding Nb_6 octahedron (*157*). The size of the displacement is enough to accommodate multiple hydrogen atoms, suggesting that more than one interstitial hydrogen may reside in the cage in high-temperature phases of $HNb_6I_8I_3$. Adsorption of hydrogen into the interstitial position is unusual, and this is the only case in which an interstitial atom is implanted in a preexisting M_6 octahedron of a metal halide cluster. The uptake of hydrogen by $Nb_6I_8I_3$ increases the number of CBE from 19 to 20, and thus a decrease in the average Nb–Nb bond length is expected. However, single-crystal X-ray diffraction studies of $Nb_6I_8I_3$ and $HNb_6I_8I_3$ reveal a slight expansion of the Nb_6 cage of $HNb_6I_8I_3$ compared to the interstitial free cluster (*158*) (Table IV). By contrast, $Zr_6HCl_{12}(EtNH_2)_6$ contains interstitial hydrogen atoms but an average Zr–Zr bond length is ~0.3 Å shorter than the interstitial free $[Zr_6Cl_{12}H_5Cl_6]^{2-}$, which has a comparable CBE count (both at 13) (*159*, *160*).

Low-temperature magnetic susceptibility measurements on $Nb_6I_8I_3$ and $HNb_6I_8I_3$ reveal ground spin states of $S = 1/2$ and $S = 0$, respec-

TABLE IV

NIOBIUM–NIOBIUM BOND DISTANCES IN SOME $\{Nb_6I_8\}^{n+}$ CLUSTERS

Cluster	CBE	d(Nb–Nb) (Å)[a]	Ref.
$Nb_6I_8I_3$	19	2.850	*158*
$HNb_6I_8I_3$	20	2.890	*158*
$CsNb_6I_8I_3$	20	2.825	*155*
$Nb_6I_8(NH_2CH_3)_6$	22	2.755	*2*

[a] Average Nb–Nb bond lengths are reported with crystals at room temperature except $HNb_6I_8I_3$ (211 K).

tively. At higher temperatures the former has a ground state $S = 3/2$ and the latter $S = 1$ (*161*). The change in spin states is not due to simple transitions from the ground to excited state but a coupled electronic and structural phase change (*158*, *161*, *162*). Heat capacity, X-ray diffraction, and magnetic susceptibility measurements indicate that a second-order or higher phase change occurs at 274 K for $Nb_6I_8I_3$ and 324 K for $HNb_6I_8I_3$. The structural deformation, a rotation of one Nb_3 face of the octahedron by 7°, is accompanied by the crossing of electronic levels, which leads to a reduction of the spin degeneracy. This spin-crossover transition is made possible by competition between the effects of a spin flip and changes in the molecular orbital levels that result from the cluster distortion (*163*).

Two discrete molecular compounds containing $\{Nb_6I_8\}^{n+}$ units were obtained from reactions of $Nb_6I_8I_3$ and NH_2R (R = CH_3, C_3H_7) (*2*). The amines displace all the bridging axial iodide ligands, generating the neutral complexes $[Nb_6I_8(NH_2R)_6]$. These clusters are electron-rich with 22 CBE compared to the 19- and 20-CBE $\{Nb_6I_8\}^{n+}$ cores obtained from solid-state reactions. Consequently, the increased number of electrons available for cluster bonding orbitals results in shorter Nb–Nb distances (Table IV). Magnetic susceptibility measurements indicate that $[Nb_6I_8(NH_2CH_3)_6]$ is diamagnetic. This observation is contrary to the prediction of a half-filled e_g HOMO for a 22-CBE species with a $\{M_6Y_8\}^{n+}$ geometry.

IV. Materials Chemistry Derived from Soluble Metal Halide Clusters

A. Higher Nuclearity Clusters

Mixed metal clusters have been generated by reaction of organometallic species with ambidentate cyanide ligands and $[Mo_6Cl_8(OSO_2CF_3)_6]^{2-}$ (*41*). Both $[CpMn(CO)_2CN]^-$ and $CpRu(PPh_3)_2CN$ displace the triflate ligands of $[Mo_6Cl_8(OSO_2CF_3)_6]^{2-}$, forming the 12 metal clusters $\{Mo_6Cl_8[(\mu\text{-}CN)Mn(CO)_2Cp]_6\}^{2-}$ and $\{Mo_6Cl_8[(\mu\text{-}CN)Ru(PPh_3)_2Cp]_6\}^{4+}$, respectively. Single-crystal X-ray structure determinations on $(PPN)_2\{Mo_6Cl_8[(\mu\text{-}CN)Mn(CO)_2Cp]_6\}$ reveals that the $[CpMn(CO)_2CN]^-$ fragment is coordinated to the $\{Mo_6Cl_8\}^{4+}$ core via bridging cyanide ligands (Fig. 23). Interestingly, the electronic spectra of these mixed metal clusters show an extremely intense absorbance that most likely corresponds to a charge transfer band [possibly intervalence charge transfer from the $CpMn(CO)_2CN^-$ ligand]. The intensity of this band cannot be accounted for from a simple com-

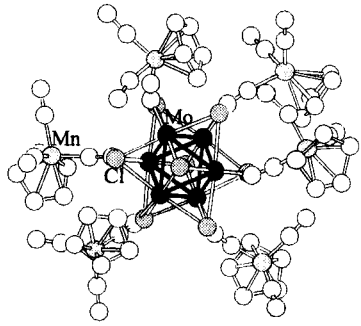

FIG. 23. Structure of $\{Mo_6Cl_8[(\mu\text{-CN})CpMn(CO)_2]_6\}^{2-}$.

bination of the absorbencies of the manganese centers and the $\{Mo_6Cl_8\}^{4+}$ core; however, "intensity-stealing" between a Mo_6-based d–d* transition and a charge transfer band may lead to the increased absorption (Fig. 24).

Cyclic voltammetry on $[Bu_4N]_2\{Mo_6Cl_8[(\mu\text{-CN})Mn(CO)_2Cp]_6\}$ reveals a broad redox wave assigned to the oxidation of the pendant manganese centers. This wave is anodically shifted 0.26 V from the "free" ligand/metal complex and is consistent with reduced electron density on the $CpMn(CO)_2$ fragment. The breadth of the redox wave is attributed to communication between the manganese and molybdenum atoms through the bridging cyanide ligands. Chemical oxidation of $\{Mo_6Cl_8[(\mu\text{-CN})Mn(CO)_2Cp]_6\}^{2-}$ with NO^+ results in clean substitution of one of the carbonyls of the manganese fragment by NO^+, generating $\{Mo_6Cl_8[(\mu\text{-CN})Mn(CO)(NO)Cp]_6\}^{4+}$.

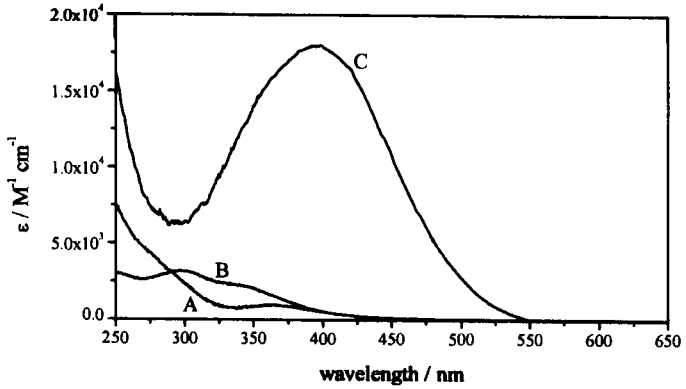

FIG. 24. Absorption spectra of **(A)** $[Bu_4N][CpMn(CO)_2CN]$, **(B)** $[Bu_4N]_2[Mo_6Cl_8(OSO_2CF_3)_6]$, and **(C)** $[Bu_4N]_2\{Mo_6Cl_8[(\mu\text{-CN})CpMn(CO)_2]_6\}$ in CH_2Cl_2.

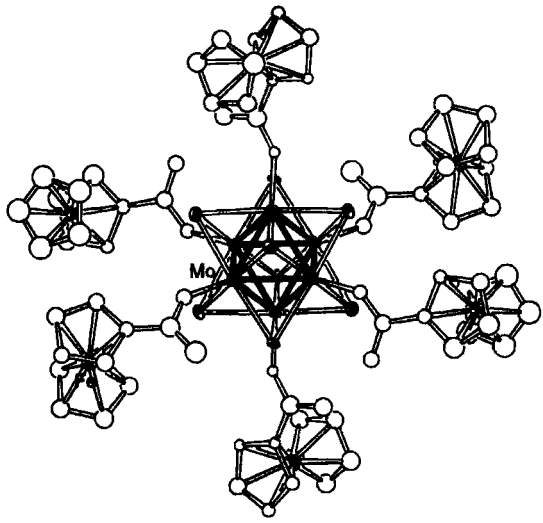

FIG. 25. Structure of $[Mo_6Cl_8(O_2CC_5H_4FeCp)_6]^{2-}$.

Reaction of $Na_2Mo_6Cl_8(OCH_3)_6$ with the carboxylic acid $HO_2CC_5H_4FeCp$ produces the organometallic derivative $Na_2Mo_6Cl_8(O_2CC_5H_4FeCp)_6$ (*55*). The iron centers are attached to the $\{Mo_6Cl_8\}^{4+}$ core through the carboxylate moieties on the Cp ring (Fig. 25). In contrast to voltammograms of $\{Mo_6Cl_8[(\mu\text{-}CN)Mn(CO)_2Cp]_6\}^{2-}$, cyclic voltammograms of $Na_2Mo_6Cl_8(O_2CC_5H_4FeCp)_6$ in DMF display a single redox wave shifted 0.10 V from that of the acid $HO_2CC_5H_4FeCp$, indicating that the iron centers are independent and equivalent. Cyclic voltammetry on $Na_2Mo_6Cl_8(O_2CC_5H_4FeCp)_6$ in DMSO reveals a chemically irreversible oxidation of the iron centers. A reduction wave is observed substantially shifted to negative potentials. This chemical irreversibility is attributed to reduction of uncoordinated ferrocenium carboxylate. A decrease in basicity of the carboxylate moiety upon oxidation of the pendant ferrocenyl group should make this oxidized ligand a weaker donor, which is susceptible to dissociation. Presumably, vacant coordination sites of $\{Mo_6Cl_8\}^{4+}$ are taken up by solvent molecules.

B. SUPPORTED CLUSTER MATERIALS

A number of strategies have been developed to generate composite materials by the incorporation of the $\{Mo_6Cl_8\}^{4+}$ unit into a host ma-

trix. Coordinating polymers such as poly(4-vinylpyridine) (PVP) provide sites to bind the $\{Mo_6Cl_8\}^{4+}$ units directly to the polymer backbone. Thus, the addition of Mo_6Cl_{12} or $[Bu_4N]_2[Mo_6Cl_8(OSO_2CF_3)_6]$ to PVP in ethanol secures the $\{Mo_6Cl_8\}^{4+}$ unit to the pyridine moieties of the polymer. Because the $\{Mo_6Cl_8\}^{4+}$ unit acts as a cross-linking agent, the nature of the axial ligands on $\{Mo_6Cl_8\}^{4+}$ influences the physical properties of the cluster/polymer composite material (*164*). Dissolution of Mo_6Cl_{12} in ethanol generates $Mo_6Cl_8Cl_4(EtOH)_2$, with two labile axial sites capable of coordinating pyridine. In contrast $[Bu_4N]_2[Mo_6Cl_8(OSO_2CF_3)_6]$ has six sites available for pyridine to bind and thus provides a more effective cross-linker. The number of accessible coordination sites is reflected in the glass transition temperature, T_g, of the resulting material. Adsorption of Mo_6Cl_{12} and $[Bu_4N]_2[Mo_6Cl_8(OSO_2CF_3)_6]$ into PVP in a ratio that provides equal donor groups to cluster binding sites results in composite materials with a higher T_g than those derived from Mo_6Cl_{12}. Immobilization of the $\{Mo_6Cl_8\}^{4+}$ core by the PVP does not drastically alter the emission spectrum of the $\{Mo_6Cl_8\}^{4+}$ core; however, increasing the number of pyridine groups coordinated to the cluster lowers the excited-state lifetime (*164*). The photocatalytic properties of these materials have been demonstrated, and singlet oxygen generated by quenching the excited cluster with O_2 has been used to oxidize alkenes (*165*).

DiSalvo and co-workers developed a monomer in solvent strategy for preparing monodispersed $\{Mo_6Cl_8\}^{4+}$ units in a polymer matrix (*166*). By dissolving $[Bu_4N]_2[Mo_6Cl_8(OSO_2CF_3)_6]$ in a coordinating solvent with a polymerizable functional group such as *N*-vinylimidazole (NVI), a monomer unit containing the $\{Mo_6Cl_8\}^{4+}$ unit is generated, $[Mo_6Cl_8(NVI)_6](OSO_2CF_3)_4$. The low solubility of these tetracationic clusters is circumvented by using the monomer unit, in this case NVI, as the solvent. Polymerization of the cluster/monomer solution produces a monodispersed cluster in an organic matrix. In addition to solvating the cluster cations, the uncoordinated monomer/solvent dilutes the highly cross-linking clusters. By adjusting the cluster concentration in the monomer/solvent, the degree of cross-linking can be controlled.

Oxide supports have also been used to immobilize $\{Mo_6Cl_8\}^{4+}$ clusters with various degrees of success. Basic and acidic silica adsorb $[Bu_4N]_2[Mo_6Cl_8Cl_6]$ and $[Bu_4N]_2[Mo_6Cl_8(OSO_2CF_3)_6]$ (*167*). Both electrostatic and covalent binding of the $\{Mo_6Cl_8\}^{4+}$ core to the silica surface can be obtained with proper choice of cluster, solvent, and silica treatment. The photophysical and photocatalytic properties of the cluster are retained on the SiO_2 support (*168*).

Intercalation of the aqua complex $[Mo_6Cl_8(H_2O)_6]^{4+}$ into layered sodium montmorillonite creates a pillared structure (*169*). The cluster cations increase the d-layer spacing from 12.5 Å for sodium montmorillonite to 16.6 Å for the intercalated composite material. The driving force for the intercalation process is attributed to ion exchange with the Na^+ of the montmorillonite; however, the amount of cluster adsorbed by the layered clay is larger than expected based on the sodium content. Similar observations have been made for the intercalation of $\{Nb_6Cl_{12}\}^{2+/3+}$ and $\{Ta_6Cl_{12}\}^{2+}$ into sodium montmorillonite, which results in an increase in d-layer spacing and adsorption of excess cluster (*170*). The axial ligands attached to the intercalated group 5 clusters were not unambiguously identified, thus the driving force for intercalation is unclear.

C. Charge-Transfer Salt Complexes

Organic–inorganic charge-transfer salt complexes containing radical organic cations such as tetrathiafulvalenium $(TTF)^+$ or tetramethyltetrathiafulvalenium $(TMTTF)^+$ and anionic clusters $[M_6Cl_8Cl_6]^{2-}$ and $[M_6Cl_{12}Cl_6]^{(6-n)-}$ as counterions have been electrocrystallized. Other organic–inorganic salt complexes have been prepared from these organic radicals with smaller anions such as BF_4^-, PF_6^-, ReO_4^-, and SbF_6^- (*171*). Interactions between the organic radical cations, especially overlap of the HOMO of neighboring cations, can produce semiconducting, metallic, or superconducting properties in the molecular salt compounds. Using large cluster anions changes the anion/cation volume ratio, thereby forcing the cation radicals into new packing arrangements. Also, the use of radical cluster anions creates the possibility of anion–cation spin interactions.

Single crystals of the first charge-transfer salt complex containing a hexanuclear metal halide cluster, $(TMTTF)_2[Mo_6Cl_8Cl_6]$, were prepared from TMTTF and $[Et_4N]_2[Mo_6Cl_8Cl_8]$ (*172*). The structure of $(TMTTF)_2[Mo_6Cl_8Cl_6]$ consists of cation dimers with the anionic metal clusters in a distorted CsCl structure (Fig. 26). The CsCl arrangement is likely a consequence of the comparable volumes of the cation dimer and $[Mo_6Cl_8Cl_6]^{2-}$. Interdimer distances (S···S distance of 4.87 Å) are quite large, resulting in an insulating material. As expected no ESR signal could be obtained because the cation radicals are paired.

The tetrakis(methylthio)tetrathiafulvalenium $(CH_3S)_4TTF^+$ salt of $[Mo_6Cl_8(NCS)_6]^{2-}$ was prepared in the same manner as $(TMTTF)_2[Mo_6Cl_8Cl_6]$ and has the same CsCl-based structure with isolated dimers of $(CH_3S)_4TTF^+$ (*111*). However, unlike

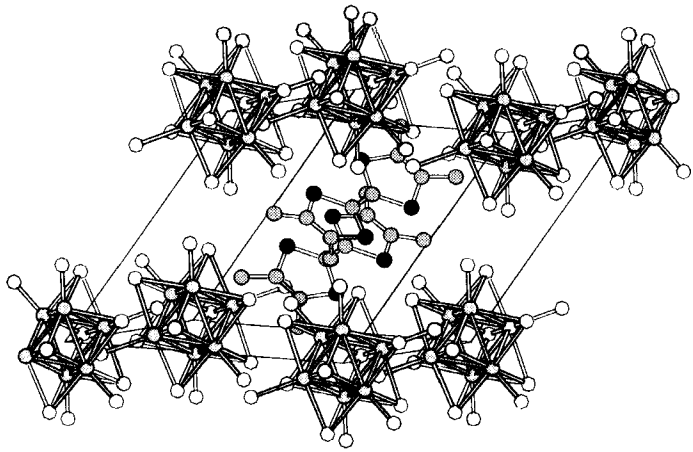

FIG. 26. Unit cell of $[TMTTF]_2[Mo_6Cl_8Cl_6]$.

$(TMTTF)_2[Mo_6Cl_8Cl_6]$, the cation dimers of $[(CH_3S)_4TTF]_2[Mo_6Cl_8(NCS)_6]$ interact with the axial ligands of the cluster. Sulfur–sulfur distances separating the $(CH_3S)_4TTF^+$ dimer and $[Mo_6Cl_8(NCS)_6]^{2-}$ are 3.793 and 3.755 Å. These cluster–cation interactions stabilize a slipped planar configuration in the cation dimer, which favors a mobile triplet exciton at room temperature. In effect, the triplet state cation dimers are coupled through the $[Mo_6Cl_8(NCS)_6]^{2-}$ cluster.

Charge-transfer salt complexes containing the ESR-active $[Nb_6Cl_{12}Cl_{12}]^{3-}$ cluster with the organic cation radicals TTF^+ and $TMTTF^+$ were prepared by electrocrystallization from CH_3CN/CH_2Cl solutions (*130*, *173*). The TTF^+ salt, which was isolated as $(TTF)_2(Bu_4N)[Nb_6Cl_{12}Cl_{12}]\cdot CH_3CN$, contains isolated TTF^+ dimers. At higher temperatures the triplet state of the cation dimer is populated and interacts with the unpaired electron localized on the $\{Nb_6CL_{12}\}^{3+}$ core. In contrast, the $TMTTF^+$ salt as well as the selenium analog TMTSF were isolated as $(TMTTF)_5[Nb_6Cl_{12}Cl_{12}]\cdot 0.5CH_2Cl$, containing a $[(TMTTF)_4]^{3+}$ cation and neutral TMTTF molecule. The TMTTF units in the $[(TMTTF)_4]^{3+}$ cation are stacked into infinite layers surrounded by $[Nb_6Cl_{12}Cl_{12}]^{3-}$ anions (Fig. 27). The fifth TMTTF molecule is neutral and orthogonal to the cationic TMTTF species. Four partially oxidized TMTTF molecules are present. The HOMO of the organic stack is 5/8 filled (5 electrons in 4 orbitals), and metallic properties are expected. Conductivity measurements, however, indicate that the hybrid material is semiconducting, with band gaps of 0.16 and 0.20 eV for the TMTTF and TMTSF, respectively. Inequivalency in

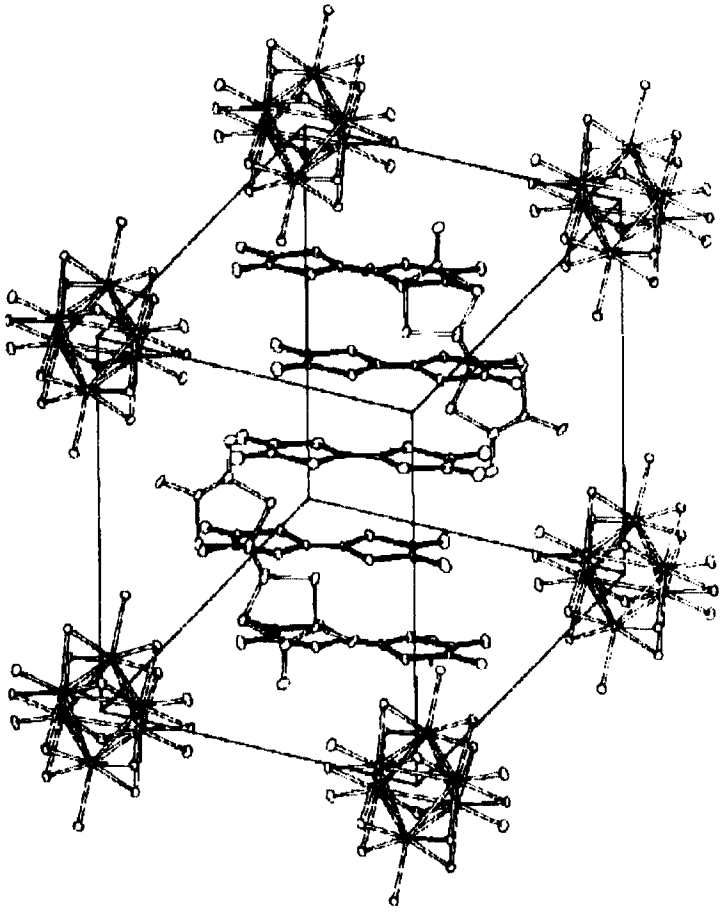

FIG. 27. Unit cell of $[TMTTF]_5[Nb_6Cl_{12}Cl_6]$; two clusters at corners of the unit cell are omitted for clarity. Reprinted with permission from Ref. (*130*).

the structures of the stacked cations is invoked to explain the electron localization and the resulting semiconducting properties. A single ESR signal is obtained for both $(TMTTF)_5[Nb_6Cl_{12}Cl_{12}]$ and $(TMTSF)_5[Nb_6Cl_{12}Cl_{12}]$, which indicates mixing of the localized spins of the cluster and cation.

D. EXTENDED SOLIDS

The most notable example of a covalently linked extended solid generated from a soluble precursor is Prussian blue (*174*). A number of strategies for assembling discrete mononuclear complexes into ex-

tended solids have been adapted to the formation of an extended metal halide cluster network. Interactions between counter cations and the ligands of the metal halide clusters often result in solids with bonding in one, two, or three dimensions. Hydrogen bonding between ligands with donor or acceptor groups and water molecules in the crystal lattice also provides intercluster linkage.

Alkali metal salts of $[M_6Y_8X_6]^{2-}$ and $[M_6Y_{12}X_6]^{(6-n)-}$ often contain cation–cluster interactions that fill the coordination sphere of the alkali metal cation. When ligands from neighboring clusters coordinate to a common cation, an extended network results. A recent example is the ferrocenecarboxylate derivative, $Na_2[Mo_6Cl_8(O_2CC_5H_4FeCp)_6]$, in which the ferrocenyl moieties are connected to the $\{Mo_6Cl_8\}^{4+}$ core through the carboxylate groups (*55*). The multidentate properties of the carboxylate group enable the ligand to coordinate to the cluster and the sodium counterions. Two carboxylate ligands from one cluster are linked to a sodium counterion, and a third ligand from an adjacent cluster anion plus a methanol molecule fill the coordination sphere of the cation. These interactions create a one-dimensional array of $[Mo_6Cl_8(O_2CC_5H_4FeCp)_6]^{2-}$ anions (Fig. 28).

Crystals of the pseudohalide complexes $AM_6Y_{12}X_6$ (A = K, Rb, Cs; Y = Cl, Br; X = N_3, NCS) produced from aqueous solutions incorporate water molecules in the unit cell (*131–133*). These water molecules as well as the inner halide and the pseudohalide ligands coordinate the alkali cations, resulting in an extended solid with a three-dimensional array. Interestingly both the α- and β-nitrogens of the azide ligand bind the cations, whereas only the sulfur atoms of the thiocyanate groups coordinate to the alkali metals. In addition to cation bridges, water molecules connect the azide ligands of adjacent clusters via hydrogen bonding.

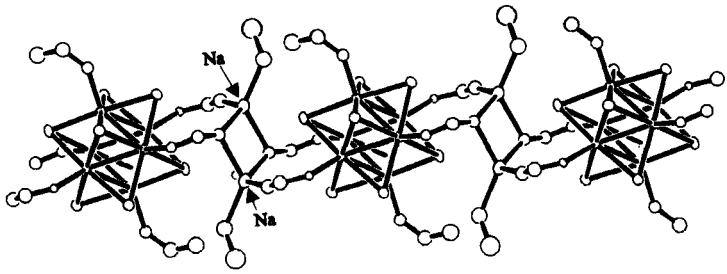

FIG. 28. Display of the linear chain of $\{Mo_6Cl_8\}^{4+}$ units connected through bridging carboxylate ligands and sodium ions of $Na_2[Mo_6Cl_8(O_2CC_5H_4FeCp)_6]$. The ferrocenyl moieties of the carboxylate groups are omitted for clarity.

Extensive hydrogen bonding has been observed in many structures containing $\{M_6Y_{12}\}^{n+}$ units with OH^-, H_2O, or CH_3OH ligands in the axial sites. The axial ligands act as both proton donors and acceptors. Hydrogen bonding interactions between the axial ligands and solvent molecules of the crystal lattice create three-dimensional cluster systems. A few structures containing extended networks of clusters linked via hydrogen bonds are listed in Table V. It should be noted that the hydrogens were not located in the structures but inferred from short donor-acceptor distances. Two compounds, $(Me_4N)[Ta_6Cl_{12}(H_2O)_6]Br_4$ (*175*) and $[Nb_6Br_{12}(H_2O)_6][HgBr_4]\cdot 12H_2O$ (*176*), possess hydrogen bonds between water donors and bromide acceptors. DC electrical measurements indicate that $[Nb_6Br_{12}(H_2O)_6][HgBr_4]\cdot 12H_2O$ has semiconducting properties; however, the origin of this conductivity is not completely understood.

E. Chemically Modified Surfaces

The affinity of the cluster anions $[Bu_4N]_3[Nb_6Cl_{12}X_6]^{3-}$(X = Cl, Br, I) for gold and silver surfaces is determined by the identity of the axial ligand X (*177*). Only $[Nb_6Cl_{12}Br_6]^{3-}$ adsorbs in a monolayer fashion on gold as determined by quartz crystal microgravimetry, X-ray photoelectron spectroscopy, and cyclic voltammetry. Redox potentials for $[Nb_6Cl_{12}Br_6]^{3-}$ adsorbed to gold are anodically shifted 0.15 V relative to the cluster in solution. This shift is consistent with the transfer of electron density from the cluster to the metal surface. By contrast no

TABLE V

Hydrogen-Bonded Cluster Complexes

Cluster	H Bonding	Ref.
$[N(CH_3)_4][Ta_6Cl_{12}(H_2O)_6]Br_4$	H···Br, H···O	*175*
$[Nb_6Br_{12}(H_2O)_6][HgBr_4]\cdot 12H_2O$	H···Br,[a] H···O	*176*
$[Ta_6Br_{12}(H_2O)_6][HgBr_4]\cdot 12H_2O$	H···Br,[a] H···O	*176*
$[Ta_6Cl_{12}(CH_3OH)_6]Br_3$	H···Br, H···O	*179*
$[Ta_6Cl_{12}(CH_3OH)_6]Br_3\cdot 4H_2O$	H···Br, H···O	*179*
$[Na_2(CH_3OH)_9][Ta_6Cl_{12}(OCH_3)_6]\cdot 3CH_3OH$	H···O[b]	*180*
trans-$[Ta_6Cl_{12}(OH)_4(H_2O)_2]\cdot 10H_2O$	H···O	*181*
$[N(CH_3)_4]_2[Ta_6Cl_{12}(OH)_6]\cdot 21H_2O$	H···O	*181*
$Na_2[Ta_6Cl_{12}(OH)_6]\cdot 16H_2O$	H···O	*181*

[a] Bromide ligands from both the cluster cation and the anion partake in hydrogen bonding.

[b] Cation and anion are involved in hydrogen bonding.

sign of niobium or chlorine is observed in the XPS spectrum of gold surfaces that were exposed to $[Bu_4N]_3[Nb_6Cl_{12}Cl_6]^{3-}$. At the other extreme, solutions of $[Bu_4N]_3[Nb_6Cl_{12}Cl_6]$ completely dissolve gold films. The increased reactivity of the clusters with the heavier halides parallels the interaction of gold with the free halide ions, where Cl^- adsorbs the weakest and I^- the strongest (*178*). Of the three clusters only $[Nb_6Cl_{12}Cl_6]^{3-}$ forms a monolayer on silver surfaces. Both $[Nb_6Cl_{12}Br_6]^{3-}$ and $[Nb_6Cl_{12}I_6]^{3-}$ dissolve silver. These findings demonstrate that halide ligands should be versatile anchors for immobilizing many types of metal complexes to metal surfaces.

Pyridine groups immobilized on gold surfaces through strong gold–sulfur interactions displace the triflate ligands of $[Ta_6Cl_{12}(OSO_2CF_3)_6]^{4-}$ and result in a immobilized monolayer of cluster on the gold surface. XPS reveals that an average of four triflate ions are replaced by the surface-bound pyridines. Dilution of the pyridine surface with coadsorbed thiolphenol, a noncoordinating moiety, reduces the amount of cluster adsorbed to the surface and the average number of triflate ligands displaced by surface pyridine. The number of triflate ligands remaining on the surface-bound cluster may be adjusted with the thiolphenol/mercaptopyridine ratio. The different coordination environments about the $\{Ta_6Cl_{12}\}^{n+}$ core in the resulting material have been identified with differential pulse voltammetry. As the number of coordinating pyridine ligands coordinated to the $\{Ta_6Cl_{12}\}^{n+}$ core decreases, the oxidation potentials of the clusters are cathodically shifted. The shift reflects the π-acid character of the pyridine ligand.

ACKNOWLEDGEMENTS

We appreciate the many contributions of former graduate students and senior collaborators, who have contributed to our research in the area of inorganic metal cluster chemistry: Laura Robinson, Dean Johnston, Joseph Hupp, and Donald Ellis. Our research in this area was supported by the National Science Foundation, inorganic chemistry program and the NSF supported Materials Research Center at Northwestern University.

REFERENCES

1. Schäfer, H.; Schnering, H.-G. v. *Angew. Chem. Int. Ed. Engl.* **1964,** *76,* 833.
2. Stollmaier, F.; Simon, A. *Inorg. Chem.* **1985,** *24,* 168.
3. Ziebarth, R. P.; Corbett, J. D. *Acc. Chem. Res.* **1989,** *22,* 256.

4. Rogel, F.; Zhang, J.; Payne, M. W.; Corbett, J. D. *Adv. Chem. Ser.* **1990,** *226,* 369.
5. Chevrel, R.; Hirrien, M.; Sergent, M. *Polyhedron* **1986,** *5,* 87.
6. Hughbanks, T.; Hoffmann, R. J. *J. Am. Chem. Soc.* **1983,** *105,* 1150.
7. Blomstrand, W. *J. Prakt. Chem.* **1859,** *77,* 88.
8. Brosset, C. *Ark. Kemi. Mineral. Geol.* **1943,** *20A,* 1.
9. Maverick, A. W.; Gray, H. B. *J. Am. Chem. Soc.* **1981,** *103,* 1298.
10. Maverick, A. W.; Najdzionek, J. S.; MacKenzie, D.; Nocera, D. G.; Gray, H. B. *J. Am. Chem. Soc.* **1983,** *105,* 1878.
11. Schäfer, H.; Schnering, H.-G. v.; Tillack, J.; Kuhnen, F.; Wöhrle, H.; Baumann, H. *Z. Anorg. Allg. Chem.* **1967,** *353,* 281.
12. Hogue, R. D.; McCarley, R. E. *Inorg. Chem.* **1970,** *9,* 1354.
13. Dorman, W. C.; McCarley, R. E. *Inorg. Chem.* **1974,** *13,* 491.
14. Zhang, X.; McCarley, R. E. *Inorg. Chem.* **1995,** *34,* 2678.
15. Drobot, D. V.; Mikhailova, L. G.; Bol'shakiv, K. A.; Sbitnev, V. L. *Russ. J. Inorg. Chem.* **1978,** *23,* 643.
16. Franolic, J. D.; Long, J. R.; Holm, R. H. *J. Am. Chem. Soc.* **1995,** *117,* 8139.
17. Jödden, K.; Schäfer, H. *Z. Anorg. Allg. Chem.* **1977,** *430,* 5.
18. Stensvad, S.; Helland, B. J.; Babich, M. W.; Jacobson, R. A.; McCarley, R. E. *J. Am. Chem. Soc.* **1978,** *100,* 6257.
19. Aufdembrink, B. A.; McCarley, R. E. *J. Am. Chem. Soc.* **1986,** *108,* 2474.
20. Zietlow, T. C.; Gray, H. B. *Inorg. Chem.* **1986,** *25,* 631.
21. Cotton, F. A.; Poli, R. *J. Am. Chem. Soc.* **1988,** *110,* 830.
22. Burini, A.; Cotton, F. A.; Czuchajowska, J. *Polyhedron* **1991,** *10,* 2145.
23. Sheldon, J. C. *J. Chem. Soc.* **1960,** 1007.
24. Sheldon, J. C. *J. Chem. Soc.* **1960,** 3106.
25. Lessmeister, P. v.; Schäfer, H. *Z. Anorg. Allg. Chem.* **1975,** *417,* 171.
26. Harder, K.; Peters, G.; Preetz, W. *Z. Anorg. Allg. Chem.* **1991,** *598/599,* 139.
27. Preetz, W.; Braack, P.; Harder, K.; Peters, G. *Z. Anorg. Allg. Chem.* **1992,** *612,* 7.
28. Fergusson, J. E.; Robinson, B. H.; Wilkins, C. J. *J. Chem. Soc. A.* **1967,** 486.
29. Carmichael, W. M.; Edwards, D. A. *J. Inorg. Nucl. Chem.* **1967,** *29,* 1535.
30. Sheldon, J. C. *J. Chem. Soc.* **1961,** 750.
31. Field, R. A.; Kepert, D. L.; Taylor, D. *Inorg. Chim. Acta* **1970,** *4,* 113.
32. Hamer, A. D.; Smith, T. J.; Walton, R. A. *Inorg. Chem.* **1976,** *15,* 1014.
33. Saito, T.; Nishida, M.; Yamagata, T.; Yamagata, Y.; Yamaguchi, Y. *Inorg. Chem.* **1986,** *25,* 1111.
34. Cotton, F. A.; Curtis, N. F. *Inorg. Chem.* **1965,** *4,* 241.
35. Schäfer, H.; Plautz, H.; Abel, H.-J.; Lademann, D. *Z. Anorg. Allg. Chem.* **1985,** *526,* 168.
36. Ehrlich, G. M.; Deng, H.; Hill, L. I.; Steigerwald, M. L.; Squattrito, P. J.; DiSalvo, F. J. *Inorg. Chem.* **1995,** *34,* 2480.
37. Perchenek, N.; Simon, A. *Z. Anorg. Allg. Chem.* **1993,** *619,* 98.
38. Schäfer, H.; Brendel, C.; Henkel, G.; Krebs, B. *Z. Anorg. Allg. Chem.* **1982,** *491,* 275.
39. Nannelli, P.; Block, B. P. *Inorg. Chem.* **1968,** *7,* 2423.
40. Johnston, D. H.; Gaswick, D. C.; Lonergan, M. C.; Stern, C. L.; Shriver, D. F. *Inorg. Chem.* **1992,** *31,* 1869.
41. Johnston, D. H.; Stern, C. L.; Shriver, D. F. *Inorg. Chem.* **1993,** *32,* 5170.
42. Preetz, W.; Harder, K.; Schnering, H. G. v.; Kliche, G.; Peters, K. *J. Alloy. Comp.* **1992,** *183,* 413.

43. Preetz, W.; Dublitz, D.; Schnering, H. G. v.; Saßmannshausen, J. *Z. Anorg. Allg. Chem.* **1994,** *620,* 234.
44. Brückner, P.; Peters, G.; Preetz, W. *Z. Anorg. Allg. Chem.* **1993,** *619,* 551.
45. Brückner, P.; Peters, G.; Preetz, W. *Z. Anorg. Allg. Chem.* **1993,** *619,* 1920.
46. Bublitz, D.; Preetz, W.; Simsek, M. K. *Z. Anorg. Allg. Chem.* **1997,** *623,* 1.
47. Simsek, M. K.; Preetz, W. *Z. Anorg. Allg. Chem.* **1997,** *623,* 515.
48. Harder, K.; Preetz, W. *Z. Anorg. Allg. Chem.* **1992,** *612,* 97.
49. Johnston, D. H. Ph.D. Thesis, Northwestern University, Evanston, 1993.
50. Ehrlich, G. M.; Warren, C. J.; Haushalter, R. C.; DiSalvo, F. J. *Inorg. Chem.* **1995,** *34,* 4284.
51. Perchenek, N.; Simon, A. *Z. Anorg. Allg. Chem.* **1993,** *619,* 103.
52. Perchenek, N.; Simon, A. *Acta Crystallogr.* **1991,** *C47,* 2354.
53. Schoonover, J. R.; Zietlow, T. C.; Clark, D. L.; Heppert, J. A.; Chisholm, M. H.; Gray, H. B.; Sattelberger, A. P.; Woodruff, W. H. *Inorg. Chem.* **1996,** *35,* 6606.
54. Nannelli, P.; Block, B. P. *Inorg. Chem.* **1969,** *8,* 1767.
55. Prokopuk, N.; Shriver, D. F. *Inorg. Chem.* **1997,** *36,* 5609.
56. Prokopuk, N.; Kennedy, V. O.; Stern, C. L.; Shriver, D. V. Unpublished results.
57. Sheldon, J. C. *Nature* **1959,** *184,* 1210.
58. Sheldon, J. C. *J. Chem. Soc.* **1964,** 1287.
59. Sheldon, J. C. *J. Chem. Soc.* **1963,** 4183.
60. Chisholm, M. H.; Heppert, J. A.; Huffman, J. C. *Polyhedron* **1984,** *3,* 475.
61. Sheldon, J. C. *J. Chem. Soc.* **1962,** 410.
62. Perrin, C.; Sergent, M.; Traon, F. L.; Traon, A. L. *J. Solid State Chem.* **1978,** *25,* 197.
63. Pilet, J. C.; Traon, F. L.; Traon, A. L.; Perrin, C.; Perrin, A.; Leduc, L.; Sergent, M. *Surf. Sci.* **1985,** *156,* 359.
64. Perrin, A.; Perrin, C.; Sergent, M. *J. Less-Common Met.* **1988,** *137,* 241.
65. Michel, J. B.; McCarley, R. E. *Inorg. Chem.* **1982,** *21,* 1864.
66. Ebihara, M.; Toriumi, K.; Saito, K. *Inorg. Chem.* **1988,** *27,* 13.
67. Ebihara, M.; Toriumi, K.; Sasaki, Y.; Saito, K. *Gazz. Chim. Ital.* **1995,** *125,* 87.
68. Xie, X.; McCarley, R. E. *Inorg. Chem.* **1997,** *36,* 4011.
69. Saito, T.; Yoshikawa, A.; Yamagata, T.; Imoto, H.; Unoura, K. *Inorg. Chem.* **1989,** *28,* 3588.
70. Hilsenbeck, S. J.; Young, V. G.; McCarley, R. E. *Inorg. Chem.* **1994,** *33,* 1822.
71. Ehrlich, G. M.; Warren, C. J.; Vennos, D. A.; Ho, D. M.; Haushalter, R. C.; DiSalvo, F. J. *Inorg. Chem.* **1995,** *34,* 4454.
72. Saito, T. *Adv. Inorg. Chem.* **1997,** *44,* 45.
73. Gray, H. B.; Maverick, A. W. *Science* **1981,** *214,* 1201.
74. Nocera, D. G.; Gray, H. B. *J. Am. Chem. Soc.* **1984,** *106,* 824.
75. Jackson, J. A.; Mussell, R. D.; Nocera, D. G. *Inorg. Chem.* **1993,** *32,* 4643.
76. Barnard, P. A.; Sun, I.-W.; Hussey, C. L. *Inorg. Chem.* **1990,** *29,* 3670.
77. Zietlow, T. C.; Nocera, D. G.; Gray, H. B. *Inorg. Chem.* **1986,** *25,* 1351.
78. Mussell, R. D.; Nocera, D. G. *Inorg. Chem.* **1990,** *29,* 3711.
79. Zietlow, T. C.; Schaefer, W. P.; Sadeghi, B.; Nocera, D. G.; Gray, H. B. *Inorg. Chem.* **1986,** *25,* 2198.
80. Schäfer, H.; Siepmann, R. *Z. Anorg. Allg. Chem.* **1968,** *357,* 273.
81. Siepmann, R.; Schnering, H. G. v. *Z. Anorg. Allg. Chem.* **1968,** *357,* 289.
82. Siepmann, R.; Schnering, H. G. v.; Schäfer, H. *Angew. Chem. Int. Ed. Engl.* **1967,** *6,* 637.
83. Kepert, D. L.; Marshall, R. E.; Taylor, D. *J. C. S. Dalton Trans.* **1974,** 506.

84. Ebihara, M.; Isobe, K.; Sasaki, Y.; Saito, K. *Inorg. Chem.* **1992,** *31,* 1644.
85. Zietlow, T. C.; Hopkins, M. D.; Gray, H. B. *J. Solid State Chem.* **1985,** *57, 112.*
86. Zietlow, T. C.; Schaefer, W. P.; Sadeghi, B.; Hua, N.; Gray, H. B. *Inorg. Chem.* **1986,** *25,* 2195.
87. Mussell, R. D.; Nocera, D. G. *Polyhedron* **1986,** *5,* 47.
88. Mussell, R. D.; Nocera, D. G. *J. Am. Chem. Soc.* **1988,** *110,* 2764.
89. Jackson, J. A.; Turro, C.; Newsham, M. D.; Nocera, D. G. *J. Phys. Chem.* **1990,** *94,* 4500.
90. Cotton, F. A.; Haas, T. E. *Inorg. Chem.* **1964,** *3,* 10.
91. Kettle, S. F. A. *Theor. Chim. Acta* **1965,** *3,* 211.
92. Guggenberger, J.; Sleight, A. W. *Inorg. Chem.* **1969,** *8,* 2041.
93. Voronovich, N. S.; Korol'kov, D. V. *Zh. Strukt. Khim.* **1971,** *13,* 458.
94. Voronovich, N. S.; Korol'kov, D. V. *Zh. Strukt. Khim.* **1971,** *12,* 613.
95. Müller, H. *Z. Phys. Chem. (Leipzig)* **1972,** *249,* 1.
96. Wirsich, J. *Theor. Chim. Acta* **1974,** *34,* 67.
97. Cotton, F. A.; Stanley, G. G. *Chem. Phys. Lett.* **1978,** *58,* 450.
98. Bursten, B. E.; Cotton, F. A.; Stanley, G. G. *Isr. J. Chem.* **1980,** *19,* 132.
99. Seifert, G.; Großmann, G.; Müller, H. *J. Mol. Struct.* **1980,** *64,* 93.
100. Hughbanks, T.; Hoffmann, R. *J. Am. Chem. Soc.* **1983,** *105,* 1150.
101. Wooley, R. G. *Inorg. Chem.* **1985,** *24,* 3519.
102. Hughbanks, T. *Inorg. Chem.* **1986,** *25,* 1492.
103. Robinson, L. M.; Bain, R. L.; Shriver, D. F.; Ellis, D. E. *Inorg. Chem.* **1995,** *34,* 5588.
104. Lin, Z.; Williams, I. D. *Polyhedron* **1996,** *15,* 3277.
105. Cotton, F. A. *Acc. Chem. Res.* **1969,** *2,* 240.
106. Corbett, J. D. *Acc. Chem. Res.* **1981,** *14,* 239.
107. Simon, A. *Angew. Chem. Int. Ed. Engl.* **1988,** *27,* 159.
108. Hughbanks, T. *Prog. Solid State Chem.* **1989,** *19,* 329.
109. Cotton, F. A.; Hughbanks, T.; Runyan Jr., C. E.; Wojtczak, W. A. In "Early Transition Metal Clusters with pi-Donor Ligands"; Chisholm, M. H., Ed.; VCH Publishers, Inc.: New York, 1995.
110. Brückner, P.; Preetz, W.; Pünjer, M. *Z. Anorg. Allg. Chem.* **1997,** *623,* 8.
111. Guirauden, A.; Johannsen, I.; Batail, P.; Coulon, C. *Inorg. Chem.* **1993,** *32,* 2446.
112. Weissenhorn, R. G. Z. v. *Anorg. Allg. Chem.* **1976,** *426,* 159.
113. Clark, R. J. H.; Kepert, D. L.; Nyholm, R. S.; Rodley, G. A. *Spectrochim. Acta* **1966,** *22,* 1697.
114. Cotton, F. A.; Wing, R. M.; Zimmerman, R. A. *Inorg. Chem.* **1967,** *6,* 11.
115. Zelverte, A.; Mancour, S.; Caillet, P. *Spectrochim. Acta* **1986,** *42A,* 837.
116. Mancour, S.; Potel, M.; Caillet, P. *J. Mol. Struct.* **1987,** *162,* 1.
117. Mancour, S.; Caillet, P.; Jouan, M.; Dao, N. Q. *J. Raman Spect.* **1987,** *18.*
118. Vaughan, P. A.; Sturdivant, J. H.; Pauling, L. *J. Am. Chem. Soc.* **1950,** *72,* 5477.
119. Koknat, F. W.; Parsons, J. A.; Vongvusharintra, A. *Inorg. Chem.* **1974,** *13,* 1699.
120. Recheweg, O.; Meyer, H.-J. *Z. Krist.* **1996,** *211,* 396.
121. Ueno, F.; Simon, A. *Acta Crystallogr.* **1985,** *C41,* 308.
122. McCarley, R. E.; Hughes, B. G.; Cotton, F. A.; Zimmerman, R. *Inorg. Chem.* **1965,** *4,* 1491.
123. Espenson, J. H.; McCarley, R. E. *J. Am. Chem. Soc.* **1966,** *88,* 1063.
124. Espenson, J. H. *Inorg. Chem.* **1968,** *4,* 631.
125. Espenson, J. H.; Boone, D. J. *Inorg. Chem.* **1968,** *4,* 636.
126. Eisenbraun, R.; Schäfer, H. *Z. Anorg. Allg. Chem.* **1985,** *530,* 222.

127. Cooke, N. E.; Kuwana, T.; Espenson, J. *Inorg. Chem.* **1971,** *10,* 1081.
128. Quigley, R.; Barnard, P. A.; Hussey, C. L.; Seddon, R. *Inorg. Chem.* **1992,** *31,* 1255.
129. Hussey, C. L.; Quigley, R.; Seddon, K. R. *Inorg. Chem.* **1995,** *34,* 370.
130. Pénicaud, A.; Batail, P.; Coulon, C.; Canadell, E.; Perrin, C. *Chem. Mater.* **1990,** *2,* 123.
131. Meyer, H.-J. *Z. Anorg. Allg. Chem.* **1995,** *621,* 921.
132. Reckeweg, O.; Meyer, H.-J. *Z. Naturforsch* **1995,** *50b,* 1377.
133. Reckeweg, O.; Meyer, H.-J. *Z. Anorg. Allg. Chem.* **1996,** *622,* 411.
134. Klendworth, D. D.; Walton, R. A. *Inorg. Chem.* **1981,** *20,* 1151.
135. Imoto, H.; Hayakawa, S.; Morita, N.; Saito, T. *Inorg. Chem.* **1990,** *29,* 2007.
136. Koknat, F. W.; McCarley, R. E. *Inorg. Chem.* **1972,** *11,* 812.
137. Kashta, A.; Brničević, N.; McCarley, R. E. *Polyhedron* **1991,** *10,* 2031.
138. Brničević, N.; Planinić, P.; Bašic, I.; McCarley, R. E.; Rutar, V.; Xie, X. *Inorg. Chem.* **1993,** *32,* 3786.
139. Brničević, N.; Muštović, F.; McCarley, R. E. *Inorg. Chem.* **1988,** *27,* 4532.
140. Brničević, N.; Schäfer, H. *Z. Anorg. Allg. Chem.* **1978,** *441,* 219.
141. Brničević, N.; Mesarić, S.; Schäfer, H. *Croat. Chem. Acta* **1984,** *57,* 529.
142. Hughes, B. G.; Meyer, J. L.; Fleming, P. B.; McCarley, R. E. *Inorg. Chem.* **1970,** *9,* 1343.
143. Fleming, P. B.; Dougherty, T. A.; McCarley, R. E. *J. Am. Chem. Soc.* **1967,** *89,* 159.
144. Koknat, F. W.; McCarley, R. E. *Inorg. Chem.* **1974,** *13,* 295.
145. Field, R. A.; Kepert, K. L.; Robinson, B. W.; White, A. H. *J. C. S. Dalton Trans.* **1973,** 1858.
146. Kennedy, V. O.; Stern, C. L.; Shriver, D. F. *Inorg. Chem.* **1994,** *33,* 5967.
147. Bond, M. R.; Hughbanks, T. *Inorg. Chem.* **1992,** *31,* 5015.
148. Mackay, R. A.; Schneider, R. F. *Inorg. Chem.* **1967,** *6,* 549.
149. Perrin, C.; Ihmaïne, S.; Sergent, M. *New J. Chem.* **1988,** *12,* 321.
150. Schneider, R. F.; Mackay, R. A. *J. Chem. Phys.* **1968,** *48,* 843.
151. Fleming, P. B.; McCarley, R. E. *Inorg. Chem.* **1970,** *9,* 1347.
152. Robbins, D. J.; Thomson, A. J. *J. C. S. Dalton Trans.* **1972,** 2350.
153. Bateman, L. R.; Blount, J. F.; Dahl, L. F. *J. Am. Chem. Soc.* **1966,** *88,* 1082.
154. Simon, A.; Schnering, H.-G.; Schäfer, H. *Z. Anorg. Allg. Chem.* **1967,** *355,* 295.
155. Imoto, H.; Corbett, J. D. *Inorg. Chem.* **1980,** *19,* 1241.
156. Simon, A. *Z. Anorg. Allg. Chem.* **1967,** *355,* 311.
157. Fitch, A. N.; Barrett, S. A.; Fender, B. E. F.; Simon, A. *J. C. S. Dalton Trans.* **1984,** 501.
158. Imoto, H.; Simon, A. *Inorg. Chem.* **1982,** *21,* 308.
159. Rogel, F.; Corbett, J. D. *J. Am. Chem. Soc.* **1990,** *112,* 8198.
160. Chen, L.; Cotton, F. A. *Inorg. Chem.* **1996,** *35,* 7364.
161. Finley, J. J.; Camley, R. E.; Vogel, E. E.; Zevin, V.; Gmelin, E. *Phys. Rev. B* **1981,** *24,* 1323.
162. Finley, J. J.; Nohl, H.; Vogel, E. E.; Imoto, H.; Camley, R. E.; Zevin, V.; Andersen, O. K.; Simon, A. *Phys. Rev. Lett.* **1981,** *46,* 1472.
163. Nohl, H.; Anderson, O. K. *Int. Phys. Conf. Ser.* **1980,** *No. 55,* 61.
164. Robinson, L. M.; Shriver, D. F. *Coord. Chem. Rev.* **1996,** *37,* 119.
165. Jackson, J. A.; Newsham, M. D.; Worsham, C.; Nocera, D. G. *Chem. Mater.* **1996,** *8,* 558.
166. Golden, J. H.; Deng, H.; DiSalvo, F. J.; Frechet, J. M.; Thompson, P. M. *Science* **1995,** *268,* 1463.
167. Robinson, L. M.; Lu, H.; Hupp, J. T.; Shriver, D. F. *Chem. Mater.* **1995,** *7,* 43.

168. Robinson, L. M. Ph. D. Thesis, Northwestern University, Evanston, 1995.
169. Christiano, S. P.; Pinnavaia, T. J. *J. Solid State Chem.* **1986,** *64,* 232.
170. Christiano, S. P.; Wang, J.; Pinnavaia, T. J. *Inorg. Chem.* **1985,** *24,* 1222.
171. Ouahab, L. *Chem. Mater.* **1997,** *9,* 1909.
172. Ouahab, L.; Batail, P.; Perrin, C.; Garrigou-Lagrange, C. *Mater. Res. Bull.* **1986,** *21,* 1223.
173. Pénicaud, A.; Batail, P.; Davidson, P.; Levelut, A.-M.; Coulon, C.; Perrin, C. *Chem. Mater.* **1990,** 2, 117.
174. Keggin, J. F.; Miles, F. D. *Nature* **1936,** *137,* 577.
175. Brničević, N.; Ruzic-Toros, Z.; Kojic-Prodic, B. *J. C. S. Dalton Trans.* **1985,** 455.
176. Vojnovic, M.; Antolic, S.; Kojic-Prodic, B.; Brnicevic, N.; Miljak, M.; Aviani, I. *Z. Anorg. Allg. Chem.* **1997,** *623,* 1247.
177. Prokopuk, N.; Shriver, D. F. *Chem. Mater.* **1998,** *10,* 10.
178. Deakin, M. R.; Li, T. T.; Melroy, O. R. *J. Electroanal. Chem.* **1988,** *243,* 343.
179. Brničević, N.; Nöthig-Hus, D.; Kojić-Prodić, B.; Ruzic-Toros, Z.; Danilović, Z.; McCarley, R. E. *Inorg. Chem.* **1992,** *31,* 3924.
180. Brničević, N.; McCarley, R. E.; Hilsenbeck, S.; Kojić-Prodić, B.; *Acta Crystallogr.* **1991,** *C47,* 315.
181. Beck, U.; Simon, A.; Širac, S.; Brničević, N.; *Z. Anorg. Allg. Chem.* **1997,** *623,* 59.